

## **Geochemical and geological constraints on the composition of marine sediment pore fluid: possible link to gas hydrate deposits**

A. Mazumdar\*, H.M. João, A. Peketi, P. Dewangan, M. Kocherla, R. K. Joshi, T. Ramprasad

<sup>1</sup>National Institute of Oceanography, Dona Paula,  
Goa-403004, India

*\*for correspondence: [maninda@nio.org](mailto:maninda@nio.org)*

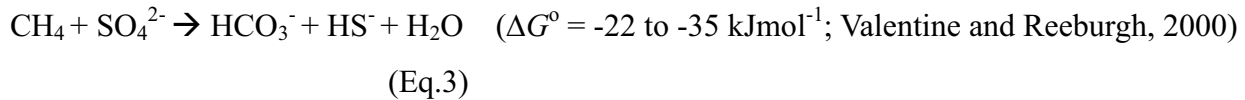
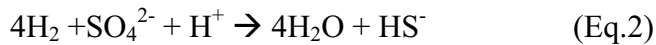
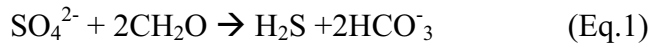
### **Abstract**

Pore water sulfate consumption in marine sediments is controlled by microbially driven sulfate reduction via organo-clastic and methane oxidation processes. In this work, we present sediment pore fluid compositions of 10 long sediment cores and high resolution seismic data from the Krishna-Godavari (K-G) basin, Bay of Bengal. Our results show occurrence of transient (S and kink types) and steady state (quasi-linear) sulfate concentration profiles which are attributed partly to the anaerobic oxidation of methane ( $\delta^{13}\text{C}_{\text{CH}_4}$ : -84.8 to -100.1 ‰VPDB) and organo-clastic sulfate reduction. Influence of AOM on alkalinity is evident from the presence of authigenic carbonate layers with highly depleted carbon isotope ratios in core MD161-8. The authigenic carbonates represent the paleo-SMTZs and suggest marked fluctuation in vertical methane flux. Our geophysical data show the acoustic signatures of upward fluid migration from shallow subsurface, whereas, coring during NGHP expedition-01 confirms the presence of subsurface gas hydrate deposits in K-G basin which can be linked to deep methane sources. The geochemical analysis suggests that shallow methane source can be attributed to high burial flux of labile organic matter due to high sedimentation rate. Sampling sites with high methane flux from the shallow gas source are characterized by quasi-linear sulfate concentration profile and a shallow sulfate methane transition zone (SMTZ) and may not be necessarily linked to deeper gas hydrate deposits. In contrast, the deep methane source results in a transient kink type sulfate profile and a deeper SMTZ. We have observed a close link between the occurrence of gas hydrate and the S/ kink type sulfate profile. We interpret the short lived 'kink' in the sulfate profiles as a result of recent enhancement in vertical methane flux possibly driven by reactivation of fault-fractures systems which provide the conduits for fluid flow.

**Keywords:** AOM, Krishna-Godavari basin, sulfate reduction, sulfate profile, SMTZ

## 1. Introduction

The composition of the liquid and gaseous phases in the marine sediments are controlled by various geological (depositional and structural) and biogeochemical processes which are closely interlinked. Abundance of labile organic matter in the sediments drives the biogeochemical cycles. The burial flux of metabolizable organic matter fueling the microbially mediated reactions depends on the oxygen exposure time, which in turn is controlled by sedimentation rate, bioturbation, organic flux and water column oxygen availability (Hedges and Keil, 1995; Hartnett et al., 1998; Gélinas et al., 2001). Evolution of sediment pore fluid composition during burial is governed by suboxic/anoxic microbial reactions like reduction of nitrate, iron, manganese, sulfate, CO<sub>2</sub> and oxidation of sulfide and methane (Schulz and Zabel, 2000). Microbial sulfate reduction (Eqs.1-2) accounts for the bulk of the organic matter mineralization in marine sediments through anaerobic pathways (Jørgensen, 1977; Jørgensen, 1982; Canfield, 1989; Kristensen, 2000).



Free energy yield ( $\Delta G^0$ ) during sulfate reduction depends on the electron donors (substrate). Fermentation products like acetate, lactate, formate and H<sub>2</sub> are the common substrates in organic rich sediments. Brüchert (2004) compiled a range of  $\Delta G^0$  values (-45 to -340 kJmol<sup>-1</sup> SO<sub>4</sub><sup>2-</sup>) for a wide range of substrates. Dissimilatory sulfate (SO<sub>4</sub><sup>2-</sup>) reduction (Harrison and Thode, 1958; Canfield, 2001; Megoñigal et al. 2003; Canfield et al., 2005b) is a bacterially-mediated metabolic process which results in the breakdown of S-O bonds of dissolved sulfate and subsequent production of H<sub>2</sub>S. During this transition, the valence state of sulfur changes from +6 to -2, i.e., a net transfer of 8 electrons via enzymatic pathways (Canfield, 2001). Sulfate reducing bacteria (SRB) are most active close to the sediment water interface owing to high labile organic load and sulfate flux at the interface (Kasten and Jørgensen, 2000; Megoñigal et al., 2003). Rate of sulfate reduction in marine sediments depends mainly on the availability of labile organic compounds which serve as substrate for SRBs (Madigan et al.,

2000), temperature (Westrich and Berner, 1988; Canfield et al., 2006), bacterial species (Canfield, 2001; Detmers et al., 2001), sedimentation rate (Goldhaber and Kaplan, 1975; Berner, 1978; Canfield 1989; Claypool, 2004), sulfate concentrations (Canfield, 2005b) and possibly bioturbation.

Other than organo-clastic sulfate reduction, microbially driven anaerobic oxidation of methane (AOM: Eq. 3) profoundly contributes towards sulfate consumption (Borowski et al., 1996, 1999; Niewohner et al., 1998). AOM is performed by a syntrophic consortium of methanotrophic archaea and sulfate-reducing bacteria (Boetius et al., 2000; Reeburgh, 2007; Orphan et al., 2001; Knittel and Boetius, 2009). Environmental genomic and proteomic studies (Krüger et al., 2003; Hallam et al., 2004; Scheller et al., 2010) suggest strong phylogenetic link between the methanogens and methanotrophic archaea (ANME I and II). AOM prevents the release of methane into the atmosphere from ocean sediments, which would otherwise cause a major increase in green house gas concentrations (Lashof and Ahuja, 1990). AOM consumes >90% of the total methane produced (85-300 Tg CH<sub>4</sub> year<sup>-1</sup>) annually in the oceanic sediments (Hinrichs and Boetius, 2002; Reeburgh, 2007). The zone within anoxic sediment column where pore water sulfate and methane concentration profiles intersect and are depleted to non detectable concentrations is known as the sulfate-methane transition zone (SMTZ). High methane flux in the sediment may also lead to enhanced methane saturation promoting gas hydrate formation under suitable temperature-pressure conditions (Kvenvolden, 1993; Sloan, 1998). Methane hydrate is an ice like crystalline solid in which methane and other lighter hydrocarbon gases are trapped inside a cage like structure of water molecules (Sloan, 1998). Attempts have been made to use methane flux, nature of sulfate profile and the depth to the SMTZ as tools for gas hydrate exploration (Borowski et al., 1996; 1999; Bhatnagar et al., 2008).

Methane flux profoundly influences the alkalinity and sulfate concentration profiles in the sediment column, whereas, the methanogenic pathway (thermogenic/ biogenic) controls the isotopic composition of dissolved inorganic carbon (DIC). Focussed sulfate consumption and alkalinity production within SMTZ leads to precipitation of authigenic carbonates with markedly depleted carbon isotope ratios (Hovland et al., 1985; Ussler III and Paull, 2008).

In the Krishna-Godavari (K-G) basin, Bay of Bengal, seismic data show regional presence of bottom simulating reflector (BSR) (Ramana et al., 2007; Collett et al., 2008). Drilling and logging

activities onboard JOIDES *Resolution* in the Indian continental margins, under the aegis of Indian national gas hydrate program (NGHP) confirmed the existence of gas hydrate deposits in the K-G basin at selected locations. BSR is believed to appear due to the acoustic impedance contrast between the overlying gas hydrate deposit and the underlying free gas layer. BSR may also form due to the presence of small amount of free gas below the hydrate stability zone with negligible presence of gas hydrate (Hyndman and Spence, 1992). Integrated analyses of seismic and drilling data show that the gas hydrate is localized in K-G basin in spite of the regional presence of BSR and is primarily controlled by the fault/fracture formed by shale tectonism/ neotectonism (Dewangan et al., 2010). In this work, we have coupled the analyses of sediment pore fluid of long cores (20-30 m) collected in K-G basin within a water depth of 647 to 2078 m with the geophysical interpretation based on high resolution seismic data. We have attempted to explain the origin of sulfate profiles, source of methane and the possibility of using sulfate profile and the depth to SMTZ as tools for gas hydrate exploration.

## **2. Geological framework of the study area**

Krishna-Godavari basin is a pericratonic rift basin located in the Eastern Continental Margin of India (ECMI), covering an area of 28000 km<sup>2</sup> onshore and 145,000 km<sup>2</sup> offshore (Rao, 2001). The ECMI represents a passive continental margin which evolved through the break-up of eastern Gondwana landmass ~130 Ma ago when India separated from East Antarctica (Powell et al., 1988; Ramana et al., 1994; Scotese et al., 1988). The tectonic activity along the ECMI resulted in the formation of several NE-SW trending horst and graben like structures and the structural fabric is largely controlled by the direction of Precambrian structural grain (Rao, 2001; Rao and Mani, 1993; Gupta, 2006). A sediment thickness of 3 to 5 km in the onshore region and around 8 km in the offshore region have been reported by Bastia (2007) and Prabhakar and Zutshi (1993). Andhra alluvium and Godavari clay comprise the onshore and offshore deposits of Holocene-Pleistocene epochs. Detrital load to the K-G basin is brought by the Krishna and Godavari rivers. The Krishna river catchment lies between 13° to 19° 30' N latitude and 73° 23' to 80° 30' E longitude and extends over an area of 258,948 km<sup>2</sup>. The mean annual sediment transport of the Krishna and Godavari Rivers are estimated to be 67.7 and 170 × 10<sup>6</sup> ton respectively (Biksham and Subramanian, 1988; Ramesh and Subramanian, 1988).

Ramana et al. (2007) and Dewangan et al. (2010) have reported various structures in the study area (Fig. 1) formed due to shale tectonism/ neotectonism such as bathymetric mounds, deep-seated shale diapirs and toe thrust faults from the K-G offshore basin. These bathymetric mounds are commonly associated with fluid/gas migration features and show numerous fault/fracture systems which facilitate the accumulation of gas hydrate (Dewangan et al., 2010). The regional geothermal gradient in K-G basin increases with water depth (Tréhu, 2007: 30°C/km at 900 mbsl to 51°C/km at 1500 mbsl). However, local deviation from the general trend may occur due to fluid advection along the fault system (Dewangan et al., 2011).

### **3. Methodology**

#### *3.1 Geophysical and Geological*

Sub-Bottom Profiler (SBP) data was collected using a Seafalcon 11 echosounder onboard Marion Dufresne. This system produces high-resolution, zero-offset acoustic sections of the sub-surface as a function of the geographical position of the ship. The central frequency used in this system was 3.75 KHz. The high resolution single channel seismic (HRS) data was acquired using GeoSpark 10 kJ system onboard Sagar Nidhi (SN21) in K-G basin for gas hydrate studies. The HRS and SBP data were processed using seismic processing software “ProMAX” to generate enhanced seismic images. Processed multichannel seismic (MCS) reflection data acquired by Oil and Natural Gas Commission Ltd. (ONGC) have been used in the present study for the identification of BSR in K-G basin.

Porosity of the sediment was calculated from the difference in wet and dry weight of sediments. Dry weight of the sediments was measured after drying it at 105°C.

#### *3.2 Geochemical*

A giant Calypso piston corer was used on board Marion Dufresne (MD-161) for the retrieval of sediment cores off K-G basin over water depth ranging from 647 to 2078 m. Sampling locations are shown in figure-1. PVC liners of 10 cm inner diameter were used for core collection. Sub-sampling was carried out by cutting out 10 cm thick sediment slabs along with the liner at 1 or 1.5 meter intervals within one and a half hour of core retrieval. Sub-sampling for gas was carried out using a 10 ml cut-syringe from the core of the sediment slabs to minimize atmospheric contamination. Sediment was

stored in 28 ml glass vials with 10 ml of bactericide (sodium azide) and crimped immediately following nitrogen flushing. Sediment was homogenized using a vortex shaker and stored at 2°C until concentrations of hydrocarbon (CH<sub>4</sub>, C<sub>2</sub>H<sub>6</sub> and C<sub>3</sub>H<sub>8</sub>) gases in the head space were measured using a Varian Gas chromatograph (CP 3380). After sub-sampling for gas, sediment slabs were immediately transferred into thick plastic bags, filled with high purity nitrogen and heat sealed to avoid atmospheric oxygen contamination which can oxidize hydrogen sulfide or iron monosulfide. Pore water was extracted from the sediment using a Manhein type hydraulic press following standard ODP protocol. Pore waters were collected in 20 ml plastic syringes with Leur locks. They were filtered through a 0.2 micron Whatman syringe filter and stored in crimp vials under nitrogen head and preserved at 2°C. Total alkalinity was measured on-board using Gran titration method using a Metrohm Autotitrator (Titrino 799 GPT). Sulfate concentrations were measured using a Dionex-600 ion chromatograph (Gieskes et al., 1991). Prior to sample injection, 1 ml of pore water sample was diluted to 50 ml or 100 ml and passed through a silver cartridge to remove chloride ion. An IonPac AS9-HC column was used for ion separation and ASRS Ultra-II (2 mm) was used as anion self-regenerating suppressor. Calibration curve was prepared using standard IC sulfate solution from Dionex. Hydrogen sulfide concentrations were determined spectrophotometrically using H<sub>2</sub>S-NN dimethyle-p-phenylenediaminesulfate complexation method following Cline (1969).

Chloride concentrations in the pore water were determined by potentiometric titration using an auto titrator (Metrohm 799 GPT Titrino) attached with a 685 Dosimat. 0.5ml of pore water was diluted to 10ml with distilled water and titrated against 0.1M AgNO<sub>3</sub>. An indicator electrode (silver electrode) coupled with a reference electrode was used to monitor the change in electromotive force (EMF). The end point was determined by the jump in EMF. Sample reproducibility by the titration method is ±4.8 mM. Ammonia in pore waters was measured spectrophotometrically using the indophenols blue complex with Nitroprusside catalyst (Koroleff, 1976).

Carbon stable isotope ratios of head space gases were measured using a Thermo Delta V continuous flow isotope ratio mass spectrometer attached with gas chromatograph (Thermo trace GC). The external precision calculated is typically 0.07–0.09 ‰ VPDB for δ<sup>13</sup>C. Carbon isotope ratios of carbonate in bulk sediments were determined with a Thermo Delta V continuous flow isotope ratio mass spectrometer attached with a GASBENCH II equipped with a PAL autosampler. The carbon isotope ratios are

reported in standard  $\delta^{13}\text{C}$  format relative to VPDB standard. A sample reproducibility of 0.1‰ for both carbon and oxygen is reported here.

Total carbon (TC) content of sediments was measured by elemental analyzer (Thermo CNS 2500). Total inorganic carbon (TIC) content was measured by UIC carbon coulometer (CM 5130). Total organic carbon (TOC) was calculated by subtracting TIC from TC.

AMS  $^{14}\text{C}$  dates were generated at National Ocean Sciences AMS (NOSAMS) facility, Woods Hole Oceanographic Institution, USA. Dates were determined on planktonic foraminifera species *Globigerina ruber* and *Globigerina sacculifer*. Carbon dioxide generated from these foraminifera shells was reacted with catalyst to form graphite which was pressed into targets and analyzed on the accelerator along with standards and process blanks. Two primary standards used during  $^{14}\text{C}$  measurements are NBS Oxalic Acid I (NIST-SRM-4990) and Oxalic Acid II (NIST-SRM-4990C).

### 3.3 Computational

Diffusive sulfate/ methane flux ( $J_{\text{SO}_4}$ ) were calculated from concentration profiles using Fick's first law (Eq-4) assuming steady state conditions (Berner, 1980; Canfield, 1989, 1991),

$$J_{\text{SO}_4} = \phi D_s (dC/dX) \quad \text{Eq-4}$$

Where  $J$ ,  $C$  and  $\phi$  represent the depth-integrated sulfate reduction/ methane oxidation rate ( $\text{mmol m}^{-2} \text{yr}^{-1}$ ), sulfate/ methane concentration (mM) in the pore water and average sediment porosity respectively.  $dC/dX$  is the sulfate/ methane concentration gradient and  $D_s$  ( $\text{cm}^2 \text{sec}^{-1}$ ) is the molecular diffusivity corrected for tortuosity.  $D_s$  is calculated by the formula

$$D_s = D_o / [1+n (1-\phi)] \quad \text{Eq-5}$$

where  $n = 3$  for clays and silt (Iversen and Jørgensen, 1993).  $D_o$  = sulfate/ methane diffusivity in the absence of particles. Since  $D_o$  varies with temperature (water depth), we have calculated  $D_o$  at different temperatures using an empirical relation based on data set from Li and Gregory (1974). In this study, advective pore water transport (eg. Bioirrigation) or reoxidation of sulfide within the sediment have

been neglected. Assessing the error in calculation due to this limitation is beyond the scope of the present work.

## **4. Results**

### *4.1 Geological and Geophysical*

The regional time migrated multi-channel seismic profile in K-G basin (Fig. 1) in the vicinity of the Marion Dufresne cores (MD161/7-8, 10-13) is shown in figure-2f. The BSR is identified on the seismic section based on its distinctive characteristics such as mimicking the seafloor topography, showing opposite polarity compared to that of the seafloor and cross-cutting the existing geological strata. The BSR is observed below the Marion Dufresne cores MD161-8, 10, 11 and is absent below cores MD161-7, 12 and 13. Core MD161-13 is located at a water depth of 647 m which is beyond the gas hydrate stability zone for the ambient pressure-temperature conditions in K-G basin (NIO Technical report, 2005). The presence of large scale faults is observed in the seismic profile.

The detailed depositional environment of K-G offshore basin is described by Dewangan et al. (2010) based on the analysis of SBP, HRS, bathymetry and seismic data. The HRS data in the vicinity of cores MD161/12,13 show distinct surface echo with several parallel, continuous subbottom reflections that are conformable to seafloor topography and regional/counter-regional growth faults are common (Fig. 2 C). The SBP and HRS data in the vicinity of the cores MD161/7, 10, 11 (Figs. 2 E, D, A) show parallel continuous sub-bottom reflections in the upper 5-10 mbsf which are underlain by thick acoustic transparent mass having few internal reflectors (10-35 mbsf). The transition between the continuous sub-bottom reflectors and acoustic transparent masses is diffusive owing to upward movement of fluid across the thick acoustic transparent layer (zoom outs of Fig. 2 A). The acoustic signature of gas movement such as acoustic voids (Hovland and Curzi, 1989) is also observed within the layered structures of MD161-12 and MD161-13 (Fig. 3 B). Acoustic transparent masses of varying thickness (5-10 m) are observed in the vicinity of these sites at a depth of 25-30 mbsf (Fig. 3 A). The core MD161-8 is located on the top of a mound (Fig. 1) where fault/fractures are associated with gas migration features such as acoustic chimneys, acoustic voids and acoustic turbid layer (Mazumdar, et al., 2009; Dewangan, et al., 2010; Dewangan, et al., 2011). The SBP data in the vicinity of MD161-02 suggests poorly resolved layered sediment within the top (5-10 m) which is underlain by acoustic transparent masses



(Fig. 3 C). The SBP data close to MD161-01 suggests the presence of layered sediment with some faulting (Fig. 3 D). The vertical and horizontal resolutions of SBP data decreases with increasing water depth due to progressive loss in higher frequency by seismic attenuation. In addition, SBP data is poor in imaging dipping reflector at greater depth which results in poor signal quality of the SBP data in the vicinity of MD161-03 and -09 and no meaningful subsurface information can be interpreted. The thickness of the late Holocene sediment cover (Fig. 4) prominently observed in the HRS data is about 23 m at a water depth of 600 m and decreases to less than 5 m beyond 1100 m water depth resulting in a wedge shaped drape.

## 4.2 Geochemical

### 4.2.1 Sulfate-methane-alkalinity, chloride concentration profiles

Sulfate-methane-alkalinity profiles for eight sites are plotted in figure- 6A-H and sulfate-alkalinity profile for other two sites (MD161-2 and 9) are presented in figure 6I-J. The sulfate concentration profiles are grouped as kink-type (MD 161-1, 3 and 9), S-type (MD161-8) and quasi-straight type (MD161-2, 7, 10, 11, 12 and 13). In the kink type profiles, the sulfate concentration gradients differ significantly above and below the kink (Figs. 6A, B, and I). The depths at which the gradient changes, vary from 7.2 to 14.05 mbsf.  $J_{SO_4}$  above the kink ranges from 3.8 to 7.2  $\text{mmol m}^{-2}\text{y}^{-1}$ , whereas, below the kink,  $J_{SO_4}$  ranges from 19.1 to 30.6  $\text{mmol m}^{-2}\text{y}^{-1}$ . In case of S-type profile (MD161-8), three distinct sulfate gradients (Fig. 6 D) are observed within the top 15 mbsf.  $J_{SO_4}$  is 19.5  $\text{mmol m}^{-2}\text{y}^{-1}$  for the top 3 mbsf and drops to 2.3  $\text{mmol m}^{-2}\text{y}^{-1}$  within the depth zone 3 to 12 mbsf. In S-type, the kink in sulfate gradient is observed at a depth of 13 mbsf. The  $J_{SO_4}$  below the kink is 21.1  $\text{mmol m}^{-2}\text{y}^{-1}$ . The sulfate gradients for the quasi-straight type profiles vary from 0.033 to 0.049  $\text{mM/cm}$  (Figs. 6C, E, F, G, H and J). The  $J_{SO_4}$  for MD161-2, 7, 10-13 are 30.9, 31.1, 25.2, 25.6, 25.8 and 28.6  $\text{mmol m}^{-2}\text{y}^{-1}$  respectively. The depth to SMTZ for the kink and S-type sulfate profiles range from 12.5 to 19.1 mbsf. Whereas for the quasi-straight type, depth to SMTZ ranges from 5 to 10 mbsf. In the absence of methane concentration data, the depth to SMTZ for MD161-1, 2 and 9 is assumed as the depth to non-detectable sulfate concentrations. Methane concentrations increase sharply below the SMTZ and show highly variable gradients.  $J_{CH_4}$  values range widely from 2.5 to 15.2  $\text{mmol m}^{-2}\text{y}^{-1}$ . Total alkalinity (TA) profiles of MD161-1,3,9 and 8 show marked increase in gradient at a depth where sulfate concentration

gradient changes. TA profiles for MD161-2, 7,10,11,12 and 13 show an approximate parabolic shape that is symmetrical across the SMTZ. However, below this zone complex alkalinity profiles are recorded in MD161-2, 7, 10 and 11. Hydrogen sulfide was not detected in any of the cores.

Chloride (Cl<sup>-</sup>) concentrations in the cores show fluctuations within a range of 533-563 mM except in MD161-2 where the concentration drops to 522 and 527 mM at depths 23 and 33 mbsf respectively (Fig. 7). The average Cl<sup>-</sup> concentration for all the cores is 545 ± 7.7 mM. The mean sea water Cl<sup>-</sup> concentration (550 mM) is demarcated in the figure.

#### 4.2.2 Methane and CO<sub>2</sub> carbon stable isotope profiles

Carbon stable isotope ratios of CH<sub>4</sub> and CO<sub>2</sub> gases in the headspaces are plotted in figure -8. Close to the SMTZ, δ<sup>13</sup>C<sub>CH<sub>4</sub></sub> reaches minima which range from -84.8 to -100.1 ‰VPDB. The δ<sup>13</sup>C<sub>CH<sub>4</sub></sub> increases gently down depth below SMTZ and shows a parallel trend with δ<sup>13</sup>C<sub>CO<sub>2</sub></sub>. Carbon isotope ratios of CO<sub>2</sub> show enrichment with depth below SMTZ. Low δ<sup>13</sup>C<sub>CO<sub>2</sub></sub> values (-21.3 to -27.6 ‰VPDB) are recorded close to the SMTZ. Δδ<sub>CO<sub>2</sub>-CH<sub>4</sub></sub> (ε) below SMTZ ranges from 59.8 to 80.4 and show low variability at individual sites. Except at MD161-8, δ<sup>13</sup>C<sub>CH<sub>4</sub></sub> increases sharply above SMTZ and approaches δ<sup>13</sup>C<sub>CO<sub>2</sub></sub> values. The sharp increase in δ<sup>13</sup>C<sub>CH<sub>4</sub></sub> is also shown in figure- 9 which shows the variations in δ<sup>13</sup>C<sub>CH<sub>4</sub></sub> with C1/C2+C3 ratios. δ<sup>13</sup>C<sub>CO<sub>2</sub></sub> shows much less variation across the SMTZ.

#### 4.2.3 Ammonium profile and Total Organic Carbon content

At all the sites, ammonium concentrations (Fig. 10) in the pore waters increases with depth below the sediment water interface except at MD161-8 where a marked depletion is noted in the NH<sub>4</sub><sup>+</sup> concentrations within 10 to 20 mbsf.

Total organic carbon (TOC) content is well constrained between 1 to 2 wt% (Fig. 11). TOC content decreases to 1-1.2% towards the core tops (supplementary table-1). The average porosity varies from 59 to 69%.

#### 4.2.4 $\delta^{13}C$ of TIC

Carbon isotope ratios of TIC in MD161-8 (Fig. 12) varies from -43.02 to -1.06 ‰ VPDB. Most pronounced carbon isotope depletion is recorded within 8.32-11.05 mbsf and 17.05-30 mbsf. The  $\delta^{18}O_{TIC}$  varies from -4.6 to +3.9‰ VPDB. Enriched oxygen isotope ratios (>0‰) were recorded corresponding to the highly depleted carbon isotopes.

#### 4.2.5 Radiocarbon ages

Age depth curves for the five sites at K-G basin are presented in figure 5. Radiocarbon ages are converted to mean calendar ages following the calibration curve of Fairbanks et al. (2005) and the calibration software (<http://radiocarbon.ldeo.columbia.edu/research/radcarbcal.htm>). The Holocene sedimentation rates (SR) in the K-G basin are very high and vary significantly. Pre-Holocene sedimentation rates could be measured only at MD161-1 and 8. SR at MD161-1 increases steeply from 27.6 to 307 cm/ky in the top 12 mbsf during the Holocene period, whereas the pre-Holocene SR varies from 5.7 to 19.9 cm/ky (Avg:  $13.6 \pm 7.2$  cm/ky) up to 41 ky BP. At MD161-8, high SR (38.8 to 248.3 cm/ky) is recorded for the upper 7 mbsf. Below 7 mbsf, the sedimentation rate drops to 17.5 cm/ky and remains constant up to an age of 45 ky BP (Mazumdar, et al., 2009). At MD161-13, average SR is 573 cm/ky down to a depth of 22 m below which the age does not increase with depth. At MD161-7, SR is 377 cm/ky for the top 6 mbsf. Below 6 m, the age remains constant at ~ 1.5 ky. At MD161-11, SR varies from 137 to 336 cm/ky in the top 13 mbsf. The transition from layered structure to acoustically transparent masses as observed at MD161-7, 11 and 13 in the SBP profiles (Fig. 2) roughly corresponds to the abrupt breaks (Fig. 5) in SR at the depths of 6, 12 and 22 mbsf respectively.

## 5. Discussion

### 5.1 Depositional environment and fault system

The SBP data in K-G basin shows the occurrence of Holocene and pre-Holocene mass transport deposits (MTD). The MTDs are mostly confined within the mid-slope minibasin and its offshore extension is restricted by the bathymetry highs like mounds/sedimentary ridges formed due to shale tectonism/neotectonism as inferred from the onlapping truncation of MTDs on the mounds

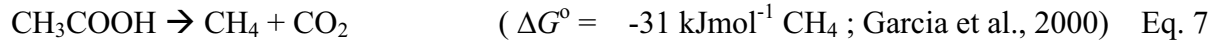
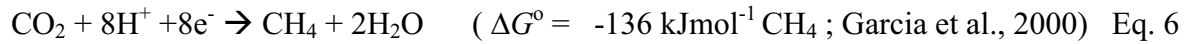
(Fig. 2B; Dewangan, et al., 2011). No evidence of gravity sliding where rigid sediment blocks slip downslope atop a decollement layer is observed in the SBP data. In the mid-slope minibasin, the MTDs are overlain by finely-layered Holocene sediment drape which pinches out with water depth (Fig. 4). The sedimentation rates of the Holocene drape covering the MTDs is very high and vary significantly from one site to another. We have not observed any evidence of exposed modern MTDs. The  $^{14}\text{C}$  age dating of the MTDs shows constant age with no variation with depth. The MTDs may be an important source of shallow gas as the rapid deposition of muddy/silty sediments would preserve the labile organic matter efficiently, which will subsequently undergo bacterial metabolization and produce gases like  $\text{CO}_2$  and  $\text{CH}_4$ . However, seismic signatures of fluid movement within the MTDs are difficult to discern due to its inherent acoustic transparency but are distinct within the layered sediments in the form of acoustic voids (Judd and Hovland, 2007). The geochemical analysis suggests that the gases are primarily composed of methane and carbon dioxide. Based on the analysis of bathymetry and high resolution seismic data, Ramprasad et al. (2011) attributed the genesis of the MTDs to the presence of high topographic gradient, high sedimentation rates in the shelf, regional fault system, shale diapirism and neotectonic activity.

The methane hydrate in K-G basin occurs within a depth of 30 to 160 mbsf (Collett, et al., 2008) suggesting the presence of deep methane source. The hydrate is primarily confined to the major and micro-fracture zones (Cook et al., 2008). The fracture/fault network enhances the porosity and permeability of the sediments thus providing the conduit for gas flow from deeper sediments. The large scale growth and toe-thrust faults in the K-G basin are the manifestation of shale tectonism (Rao and Mani, 1993; Bastia, 2007).

### *5.2 Methanogenesis and Methanotrophy*

Methane is the end product of the degradation of organic matter under anoxic condition when other electron acceptors like  $\text{NO}_3^{2-}$ ,  $\text{Mn}^{4+}$ ,  $\text{Fe}^{3+}$  or  $\text{SO}_4^{2-}$  ions are depleted (Martens and Berner, 1974; Canfield et al., 2005a). Methanogens can produce methane only in anoxic sediments owing to the instability of their F420-hydrogenase enzyme complex in the presence of  $\text{O}_2$ , nitrate or nitrite (Scönheit et al., 1981). Hydrogenotrophy and acetotrophy are the two major

pathways of methanogenesis as represented by Eqs. 6 and 7 (Alperin et al., 1992; Whiticar, 1999; Conrad, 2005).



Sulfate reduction being energetically a more favorable pathway of anaerobic metabolisms, sulfate reducers out compete methanogens for carbon substrates (eg. acetate) and H<sub>2</sub> in sulfate rich porewaters. Below the zone of sulfate reduction, hydrogenotrophy (CO<sub>2</sub> reduction) is the dominant methanogenic pathway since other methanogenic substrate, like acetate, is depleted due to organo-clastic sulfate reduction (Whiticar and Faber, 1986; Whiticar, 1999; Galimov, 2006; Conrad, 2005). Methane concentrations increase sharply below the SMTZ (Fig. 6) and show a concave upward pattern. However, down depth, the profiles show significant fluctuations due to heterogeneous distribution of gas pockets. Fluctuations in the methane concentration profiles have earlier been reported from K-G basin by Collett et al. (2008). The methane concentrations and fluxes reported in the present work are possibly much less than the in situ concentrations owing to degassing during core recovery and onboard sub-sampling (Dickens et al., 1997; Paull and Ussler III, 2001). Highly depleted carbon isotopic compositions of methane below the SMTZ (-84.8 to -100.1‰ VPDB), high C<sub>1</sub>/(C<sub>2</sub>+C<sub>3</sub>) ratios (1000-6000) and Δδ<sub>CO<sub>2</sub>-CH<sub>4</sub></sub> ranging from 59.8 to 80.4‰ indicate the microbial origin of methane in K-G basin via CO<sub>2</sub> reduction pathway (Whiticar and Faber, 1986; Whiticar, 1999; Galimov, 2006). Other factors which may influence δ<sup>13</sup>C<sub>CH<sub>4</sub></sub> include methanogenic precursor, fractionation factor, temperature etc. (Alperin et al., 1992; Whiticar, 1999). The possible contribution of acetate fermentation in methanogenesis is difficult to assess in the absence of δD<sub>CH<sub>4</sub></sub>, δ<sup>13</sup>C<sub>acetate</sub> and acetate concentration measurements (Conrad, 2005). The down depth enrichment in the carbon isotope ratio of methane may be attributed to the continued preferential removal of the isotopically lighter molecules from the carbon pool (CO<sub>2</sub>) during methanogenesis resulting in a progressive shift in the residual substrate towards enriched carbon isotope ratios following Rayleigh fractionation. The concave upward nature of methane concentration profile close to SMTZ is a result of methane consumption via AOM typically represented by Eq. 3. The upward decrease in

C1/(C2+C3) ratios (Table-1) of hydrocarbon gases suggests preferential consumption of methane at and above the SMTZ resulting in carbon isotopic enrichment of the residual methane due to preferential breakdown of  $^{12}\text{C-H}$  bond (Whiticar, 1999; Alperin et al., 1988; Whiticar, 1999). Carbon isotope separation ( $\Delta\delta_{\text{CO}_2\text{-CH}_4}$ ) between residual methane and  $\text{CO}_2$  decreases upwards in the cores owing to decrease in  $\text{CO}_2$  contribution from methane oxidation and increasing contribution of organo-clastics derived  $\text{CO}_2$  which approaches  $\delta^{13}\text{C}_{\text{TOC}}$ . The  $\delta^{13}\text{C}_{\text{TOC}}$  of K-G basin range from -14 to -22 ‰ VPDB (Mazumdar et al., 2011a). Towards the core top most enriched carbon isotope ratios are commonly recorded for  $\text{CO}_2$  due to contribution from sea water. In case of MD161-8, persistence of significantly depleted carbon isotope ratios of residual methane (-70 to -61‰ VPDB) above SMTZ suggest greater upward flux of methane across SMTZ than what could be consumed via AOM. The headspace  $\delta^{13}\text{C}_{\text{CO}_2}$  shows a shift towards depleted ratios close to SMTZ suggesting contribution from methane oxidation. The most depleted carbon isotope ratio (-27.6‰ VPDB) is recorded at MD161-10. Ussler III and Paull (2008) also recorded depleted carbon isotope ratios of headspace  $\text{CO}_2$  close to SMTZ from the northern Gulf of Mexico.

### *5.3 Total alkalinity and Ammonium trends*

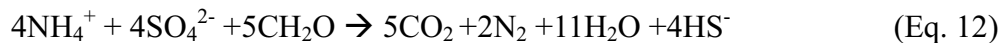
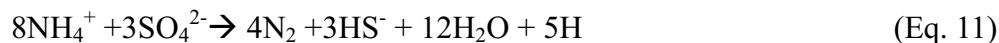
The parabolic alkalinity profiles associated with the quasi-linear sulfate concentration trends observed in MD161-2, 7, 10-13 are similar to the TA profiles reported by Kastner et al. (2008), Ussler III and Paull (2008), Schmidt et al. (2005) and believed to be typical of AOM. Vertical diffusion of bicarbonate ions produced via focused sulfate reduction at the SMTZ is apparently responsible for the parabolic TA profile (Ussler III and Paull, 2008). The role of AOM towards TA in our studied sites MD161-8 is evident from the  $\delta^{13}\text{C}_{\text{TIC}}$  data (Fig. 12). Highly depleted carbon isotope ratios indicate AOM as the bicarbonate source (Greinert et al., 2001; Chen et al., 2007). The zones of isotopically depleted TIC indicate occurrences of paleo-SMTZs (Rodriguez et al., 2000; Ussler III and Paull, 2008). The record of paleo SMTZs in the cores suggest significant fluctuations in vertical methane flux controlling the AOM process and alkalinity production. On the other hand, based on  $(\Delta\text{Ca}+\Delta\text{Alk})/\Delta\text{SO}_4^{2-}$  ratios in the porewaters from several NGHP sites, Solomon et al. (2008) showed significant contribution of organo-clastic sulfate reduction towards the alkalinity. The distribution of  $(\Delta\text{Ca}+\Delta\text{Alk})/\Delta\text{SO}_4^{2-}$  values

between 1:1 and 2:1 ratios suggest a combined contribution of bicarbonate in porewaters via AOM and organo-clastic degradation pathways (Eq.1 and 3). Additional factors like silicate weathering (Wallmann et al., 2008) and/or degassing of CO<sub>2</sub> from the sediments during core recovery and sub-sampling (Paull and Ussler III, 2001) may also lead to complicated alkalinity profiles observed in MD 161-2, 10 and 11. Alkalinity trends associated with kink type sulfate profiles show enhanced alkalinity gradient at the kink and may form a bell shaped pattern at the SMTZ as observed in MD161-9.

Ammonium is produced via anaerobic bacterial decomposition of nitrogen bearing organic compounds (Heinrich and Reeburgh, 1987). NH<sub>4</sub><sup>+</sup> production via sulfate reduction is represented by equations 8-10 (Berner et al., 1970; Heinrich and Reeburgh, 1987).



NH<sub>4</sub><sup>+</sup> concentration profile is a good indicator of availability of labile organic carbon in the sediment. High concentrations and gradient of pore water NH<sub>4</sub><sup>+</sup> in MD161-7, 10-13 relative to MD161-1, 3 and 8 suggest greater burial flux of labile organic matter (Cranston, 1991) at the former coring locations. Porewater ammonium undergoes reoxidation (Dalsgaard and Thamdrup, 2002), adsorption-desorption reaction with solid phases like clay, organic particulates and Fe-oxyhydroxides (Boatman and Murray, 1982; Mackin and Aller, 1984). The marked depletion in NH<sub>4</sub><sup>+</sup> concentrations recorded across the NH<sub>4</sub><sup>+</sup>-SO<sub>4</sub><sup>2-</sup> transition in MD161-8 may be attributed to NH<sub>4</sub><sup>+</sup> oxidation via lithotrophic (Eq. 11) and/or organotrophic (Eq.12) sulfate reducing-ammonium oxidation pathways as reported by Schrum et al. (2009) from K-G basin site NGHP-01-14A. The site specific ΔG calculated based on equation-11 is -14.6±0.2 kJ mol<sup>-1</sup> SO<sub>4</sub><sup>2-</sup>. However the low ΔG of this reaction may be difficult to sustain microbial growth.



#### *5.4 Genesis of the sulfate profiles*

The sulfate concentration profiles depend on the availability of labile organic matter amenable to sulfate reducers, diffusive/ advective methane flux and depositional conditions (Niewöhner et al., 1998; Zabel and Schulz, 2001; Hensen et al., 2003; Schmidt et al., 2005; Tréude et al., 2005; Kastner et al., 2008). Combination of these factors give rise to S, kink, concave-up, concave-down and linear type sulfate concentration trends in marine sediments. Labile organic matter availability influences the sulfate reduction rates primarily near the sediment water interface, whereas, focused sulfate consumption at the SMTZ is primarily controlled by AOM. The two maxima in the sulfate reduction rates have been reported by Iversen and Jørgensen (1985) and Tréude et al. (2005). The relative contribution of AOM on the overall sulfate concentration profile as well as the depth integrated sulfate reduction rates depend on the methane flux at the SMTZ. Sulfate flux measurements off Namibia by Niewöhner et al., (1998) showed 100% sulfate consumption at SMTZ by AOM which resulted in a linear sulfate concentration trend. Linear sulfate profiles, high concentration gradient (shallow SMTZ) and high sulfate reduction rates are expected to be coupled with high methane flux (Borowski et al., 1996; Borowski et al., 1999). The spatial variation in the linearity of sulfate profiles and depths to the SMTZ have been linked to methane hydrate occurrences (Borowski, et al., 1996; Bhatnagar, et al., 2008; Hiruta, et al., 2009). Apparently, the quasi-linear sulfate concentration profiles and high alkalinity at the SMTZ (Fig. 6) recorded from the K-G basin can be linked to high methane flux and AOM. However, significant contribution of organo-clastic sulfate reduction was shown to be associated with such quasi-linear profiles and shallow SMTZs by Solomon et al. (2008) from several NGHP sampling sites in K-G basin. Compared to the steady state linear sulfate profile, the kink type profiles suggest transient or non-steady state pore water chemistry (Hensen et al., 2003; Henkel et al., 2011). The presence of kink and overall concave up character of sulfate profiles recorded from the continental margin off Uruguay and lower Zaire (Congo) deep sea fan have been attributed to overthrusting of sediment (decollement) by cohesive slide block that carry their initial pore water characteristics on to an older strata. The kink apparently appears at the junction (surface of unconformity) of the two sulfate concentration profiles (Zabel and Schulz, 2001; Hensen et al, 2003). However, kink-type profile has also been shown to be caused by recent increase in methane flux (Borowski et al., 1999;



Halbach et al., 2004; Coffin et al., 2007; Ussler III and Paull, 2008; Mazumdar et al., 2009) with no evidence of overthrusting of slide block. Model calculations show that the kink- type transient state transforms into steady state quasi-linear form in less than 1000 years (Zabel and Schulz, 2001; Hensen et al., 2003; Halbach, 2004; Henkel et al.,2011).

Our coring sites MD161-3, MD161-8 are close to the NGHP expedition-01 drilling/coring sites NGHP-01-20 and NGHP-01-10 respectively (Collett et al., 2008). Chloride concentration measurement in cores NGHP-01-20A and NGHP-01-10D show marked freshening of pore waters suggesting thawing of methane hydrate which releases fresh water into the sediment pores thereby lowering the chloride concentrations. The zones of pore water freshening varies from 40 to 120 mbsf and 30 to 150 mbsf in NGHP-01-20A and NGHP-01-10D respectively. The Infrared (IR) anomaly of the sediment cores at these sites show cold spots attributed to thawing of hydrates. Geophysical logging data and x-ray imaging of pressure cores in site NGHP-01-10 further support the occurrence of gas hydrates. It is interesting to note that NGHP-01-10 and 20 also show kink pattern with relatively deeper SMTZ similar to that observed at sites MD161- 3 and 8. The close association of S or kink type sulfate concentration profiles with the occurrence of gas hydrate in K-G basin is further supported from pore fluid data and logging/physical characteristic of hydrate bearing sediments of cores NGHP-01-14A and NGHP-01-5C (Collett et al., 2008; Schrum et al., 2009). Both the sites show kink type sulfate profiles with depth to SMTZ ranges from 22-24 mbsf and the kink lies between 18-20 mbsf. The gentle sulfate gradients above the kink represent the steady state diffusion zone where organo-clastic sulfate reduction possibly plays the dominant role. The ammonium concentration profiles suggest relatively low burial flux of labile organic matter owing to lower sedimentation rates in contrast to the sites with shallower SMTZ. The linearly extrapolated depth to zero sulfate concentrations for the sulfate gradients above the kink would be 48, 35, 54 and 24 mbsf for MD161-1, 3, 8 and 9 respectively. The abrupt increase in sulfate and alkalinity gradients and sulfate reduction rates (J2) observed below the kink suggest AOM process driven by a likely deeper methane source. This contention is supported by the presence of major gas hydrate deposits underneath sites MD161-3 and 8.

The transient nature of the kink type sulfate profile indicates recent enhancement in methane advection. The advection of methane from deeper sedimentary layers may be facilitated by the reactivation of deep seated fault/fracture system as reported by Dewangan et al. (2011) and Riedel et al. (2010) in K-G basin. Halbach et al. (2004) suggested reactivation of faults caused by recent earthquakes as the driver for high methane flux in Marmara Basin giving rise to kink shaped sulfate trend. Focused flow of warm fluid coming from the deeper layers through fault zone may destabilize the hydrate zone and disrupt the BSR as well (Suess et al., 1999; Tomaru et al., 2007). Mazumdar et al. (2009) reported extensive methane seepage phenomenon in the K-G basin ~60-70 ky BP (Joshi, et al., *communicated*) which supported proliferation of chemosynthetic life (Mazumdar et al., 2011b). Punctuated destabilization of methane hydrate and waxing and waning of vertical flux of methane is amply evident from the record of isotopically depleted authigenic carbonate layers at MD161-8 (Fig. 12).

The sites with quasi linear sulfate profiles are characterized by significantly higher ammonium concentrations and sedimentation rates suggesting high labile organic burial flux. Higher sedimentation rate transfers the labile organic matter rapidly through the sulfate reduction zone into the methanogenic zone causing methane production at shallow burial depths. Acetotrophy may play an important role in methanogenesis where sedimentation rate is high. The vertical methane flux depends on the rate of production of methane, permeability and solubility depending on local P-T conditions. Sub-bottom profiler data in the vicinity of the coring sites (MD161-11, 12 and 13) show the presence of acoustic voids within the Holocene drape sediment suggesting upward movement of fluid through the shallow sediment layers. The acoustic voids are attributed to the presence of dissolved gas or micro-bubbles (Hovland and Curzi, 1989). Very high methane flux may lead to crystallization of hydrate within much younger sediment layers in contrast to sites with kink profiles. We have observed anomalous chloride depletion only in MD161-2 (23 and 33 mbsf) suggesting possible thawing of methane hydrate. No other sites show similar anomalous drop in chloride concentration, thus ruling out the presence of hydrate at shallow depths at any of our studied locations. However, presence of hydrate below the penetration depth cannot be ruled out.

## Conclusions

Sediment cores collected from the K-G basin over a water depth of 647 to 2078 mbsl reveal variable pore water sulfate, alkalinity and methane concentration profiles. C1/C2+C3 ratios and  $\delta^{13}\text{C}_{\text{CH}_4}$  of headspaces gases suggest microbial origin of methane in the K-G basin. We attribute the complex nature of alkalinity profiles to organo-clastic degradation, variation in methane flux, transition of SMTZ and alkalinity consumption via precipitation of carbonates and possibly silicate weathering. The S and kink type sulfate profiles represent transient states compared to the steady state quasi-linear profiles. Our findings show both shallow and deep biogenic methane sources in the K-G basin. The quasi-linear sulfate concentration profile and a shallow SMTZ suggest high methane flux likely originating from the young and rapidly deposited sediments. The genesis of high methane flux is attributed to high burial flux of labile organic matter. Except at MD161-2 we don't have unequivocal evidence of methane hydrate at shallow depths. However presence of hydrate below penetration depth cannot be ruled out. On the other hand, deep methane source leads to a transient kink type sulfate profile and a deeper SMTZ. In K-G basin, we observe a close association of short lived S or kink type sulfate concentration profiles with the occurrence of gas hydrate deposits. The transient nature of sulfate profiles suggests recent enhancement of methane flux possibly from the neotectonic activities in K-G basin which results in opening of fault/fracture conduits allowing migration of methane. We propose that the kink type sulfate profile in areas without evidence of slide block movement may indicate the occurrence of deep methane source possibly associated with gas hydrate deposits.

## Acknowledgment

We thank the directors of NIO, NIOT, NCAOR and advisor MOES for supporting this study. Head oceanography department and in-charge on-board operations of IPEV are thanked for providing onboard technical support and facilities. Sincere thanks to students of Goa University, IIT Kharagpur and project scientists of NIO, NIOT, PRL and NGRI. Research fellowship from VNJCT to A. Peketi is sincerely acknowledged. Comments and suggestions from the reviewers are sincerely acknowledged.

## References

- Alperin, M., Reeburgh, W., Whiticar, M., 1988. Carbon and hydrogen isotope fractionation resulting from anaerobic methane oxidation. *Global Biogeochemical Cycles* 2, 279-288.
- Alperin M.J., Blair N.E., Albert, D.B., Hoehler T.M., and Martens, C.S., 1992. Factors that control the stable carbon isotopic composition of methane produced in an anoxic marine sediment. *Global Biogeochemical Cycles* 6, 271-291.
- Bastia, R., 2007. *Geologic Settings and Petroleum Systems of India's East Coast Offshore Basins: Concepts and Applications*: Eastern Book Corporation, 204p.
- Berner, R.A., Scott, M.R., Thomlison, C., 1970. Carbonate alkalinity in the porewaters of the anoxic marine sediments. *Limnology Oceanography* 15, 544-549.
- Berner, R.A., 1978. Sulfate reduction and the rate of deposition of marine sediments. *Earth Planetary Science Letter* 37, 492-498.
- Berner, R.A., 1980. *Early Diagenesis: A Theoretical Approach*. Princeton University Press.
- Bhatnagar, G., Chapman, W.G., Dickens, G.R. and Dugan, B., 2008. Sulfate-methane transition as a proxy for average methane hydrate saturation in marine sediments. *Geophysical Research Letter* 35, 1-15.
- Biksham, G., Subramanian, V., 1988. Sediment transport of the Godavari River basin and its controlling factors. *Journal of Hydrology* 101, 275-290.
- Boatman, C.D., Murray, J.W., 1982. Modeling exchangeable  $\text{NH}_4^+$  adsorption in marine sediments: process and controls of adsorption. *Limnology and Oceanography* 27, 99-110.
- Boetius, A., Ravensschlag, K., Schubert, C., Rickert, D., Widdel, F., Gieseke, A., Amman, R., Joergensen, B.B., Wittie, U., Pfannkuche, O., 2000. A marine microbial consortium apparently mediating anaerobic oxidation of methane. *Nature* 407, 623-626.
- Borowski, W.S., Paull, C.K., Ussler III, W., 1996. Marine pore-water sulfate profiles indicate in situ methane flux from underlying gas hydrate. *Geology* 24, 655-658.
- Borowski, W.S., Paull, C.K., Ussler III, W., 1999. Global and local variations of interstitial sulfate gradients in deep-water, continental margin sediments: Sensitivity to underlying methane and gas hydrates. *Marine Geology* 159, 131-154.
- Brüchert, V., 2004. Physiological and ecological aspects of sulfur isotope fractionation during bacterial sulfate reduction In: Amend, J.P., Edwards K.J. and Lyons T.W.(Eds.), *Sulfur Biogeochemistry—Past and Present*. GSA Special Paper 379, pp. 1-16.
- Canfield, D.E., 1989. Sulfate reduction and oxic respiration in marine sediments: implications from organic carbon preservation in euxinic environments. *Deep Sea Research* 36, 121-138.

- Canfield, D.E., 1991. Sulfate reduction in deep sea sediments. *American Journal Science* 291, 177-188.
- Canfield, D.E., 2001. Biogeochemistry of sulfur isotopes. *Reviews in Mineralogy and Geochemistry* 43, 607-636.
- Canfield, D.E., Kristensen, E., Thamdrup, B., 2005a. The methane cycle. *Aquatic Geomicrobiology Advances in Marine Biology* 48, 383-418.
- Canfield, D., Kristensen, E., Thamdrup, B., 2005b. The sulfur cycle. *Aquatic Geomicrobiology. Advances in Marine Biology* 48, 313-381.
- Canfield, D.E., Olesen, C.A., and Cox, R.P., 2006. Temperature and its control of isotope fractionation by a sulfate-reducing bacterium. *Geochemistry Cosmochimistry Acta* 70, 548-561.
- Chen, Y., Matsumoto, R., Paull, C.K., Ussler III, W., Lorenson, T., Hart, P., Winters, W., 2007. Methane-derived authigenic carbonates from the northern Gulf of Mexico-MD02 Cruise, *Journal of Geochemical Exploration* 95, 1-15.
- Claypool, G., 2004. Ventilation of marine sediments indicated by depth profiles of pore water sulfate and  $\delta^{34}\text{S}$ . *The Geochemical Society Special Publication* 9, 59-65.
- Cline, J.D., 1969. Spectrophotometric determination of hydrogen sulfide in natural waters. *Limnology and Oceanography* 14, 454-458.
- Coffin, R., Pohlman, J., Gardner, J., Downer, R., Wood, W., Hamdan, L., Walker, S., Plummer, R., Gettrust, J., Diaz, J., 2007. Methane hydrate exploration on the mid Chilean coast: A geochemical and geophysical survey. *Journal of Petroleum Science and Engineering* 56, 32-41.
- Collett, T., Riedel, M., Cochran, J., Boswell, R., Presley, J., Kumar, P., Sathe, A., Sethi, A., Lall, M., and Sibal, V., 2008. The NGHP Expedition 01 Scientists. *Indian National Gas Hydrate Program Expedition 01 Initial Reports*.
- Conrad, R., 2005. Quantification of methanogenesis pathways using stable carbon isotope signatures: a review and a proposal. *Organic Geochemistry* 36, 739-752.
- Cook, A., Goldberg, D., 2008. Stress and gas hydrate-filled fracture distribution, Krishna-Godavari basin, India. 6th, *International Conference on Gas Hydrates*, Noida, India.
- Cranston, R.E., 1991. Sedimentation rate estimates from sulfate and ammonia gradients. *Proceedings of the Ocean Drilling Program, Scientific results*. In: Barron, J et al.(Eds.) 119, pp.401-405.
- Detmers, J., Bruchert, V., Habicht, K., Kuever, J., 2001. Diversity of sulfur isotope fractionations by sulfate-reducing prokaryotes. *Applied Environmental Microbiology* 67, 888-894.

- Dalsgaard, T., Thamdrup, B., 2002. Factors controlling anaerobic ammonium oxidation with nitrite in marine sediments. *Applied Environmental Microbiology* 68, 3802-3808.
- Dewangan, P., Ramprasad, T., Ramana, M.V., Mazumdar, A., Desa, M.A., Badasaab, F., 2010. Shale Diapirism in the continental slope region of Krishna-Godavari Basin, Bay of Bengal: implications in gas-hydrate exploration. *Journal of Marine Petroleum Geology* 27, 1628–1641.
- Dewangan, P., Sriram, G., Ramprasad, T., Ramana, M., Jaiswal, P., 2011. Fault system and thermal regime in the vicinity of site NGHP-01-10, Krishna-Godavari basin, Bay of Bengal. *Journal of Marine and Petroleum Geology* 28, 1899-1914.
- Dickens, G.R., Paull, C.K., Wallace, P., ODP Leg 164 Scientific Party, 1997. Direct measurement of in situ methane quantities in a large gas-hydrate reservoir. *Nature* 385, 426–428.
- Fairbanks, R.G., Mortlock, R.A., Chiu, T.C., Cao, L., Kaplan, A., Guilderson, T.P., Fairbanks, T.W., Bloom, A.L., Grootes, P.M., Nadeau, M.J., 2005. Radiocarbon calibration curve spanning 0 to 50,000 years BP based on paired  $^{230}\text{Th}/^{234}\text{U}/^{238}\text{U}$  and  $^{14}\text{C}$  dates on pristine corals. *Quaternary Science Reviews* 24, 1781-1796.
- Galimov, E. M., 2006. Isotope organic geochemistry. *Organic Geochemistry* 37, 1200-1262.
- Garcia, J.L., Patel, B.K.C., Ollivier, B., 2000. Taxonomic, phylogenetic, and ecological diversity of methanogenic Archaea. *Anaerobe* 6, 205-226.
- Gélinas, Y., Baldock, J.A., Hedges, J.I., 2001. Organic carbon composition of marine sediments: effects of oxygen exposure on oil generation potential. *Nature* 294, 145-148.
- Gieskes, J. M., Gamo, T., Brumsack, H., 1991, Chemical methods for interstitial water analysis aboard JOIDES Resolution: College Station, Texas, Ocean Drilling Program Technical Note no. 15, pp. 60.
- Goldhaber, M., Kaplan, I., 1975. Controls and consequences of sulfate reduction rates in recent marine sediments. *Soil Science* 119, 42-55.
- Greinert, J., Bohrmann, G., Erwin, S., 2001. Gas hydrate-associated carbonate and methane-venting at Hydrate Ridge: classification, distribution and origin of authigenic lithologies. In: Paul, C. K., Dillon, W. P. (Eds.) *Natural gas hydrate: occurrence, distribution and detection*, Geophysics Monograph 124, pp.99-113.
- Gupta, S.K., 2006. Basin architecture and petroleum system of Krishna Godavari basin, east coast of India. *The Leading Edge* 25, 830.
- Halbach, P., Holzbecher, E., Reichel, T., Moche, R., 2004. Migration of the sulphate-methane reaction zone in marine sediments of the Sea of Marmara - can this mechanism be tectonically induced? *Chemical Geology*, 205, 73-82.

- Hallam, S.J., Putnam, N., Preston, C.M., Detter, J.C., Rokhsar, D., Richardson, P.M., DeLong, E. F., 2004. Reverse methanogenesis: testing the hypothesis with environmental genomics. *Science* 305, 1457–1462.
- Harrison, A.G., Thode, H.G., 1958. Mechanism of the bacterial reduction of sulphate from isotopic fractionation studies. *Transactions of the Faraday Society* 54, 84-92.
- Hartnett, H.E., Keil, R.G., Hedges, J.L., Devol, A.H., 1998. Influence of oxygen exposure time on organic carbon preservation in continental margin sediments. *Nature* 391, 572-574.
- Hedges, J.I., Keil, R.G., 1995. Sedimentary organic matter preservation: an assessment and speculative synthesis. *Marine Chemistry*. 49, 81-115.
- Henkel, S., Strasser, M., Schwenk, T., Hanebuth, T.J.J., Hüsener, J., Arnold, G., Winkelmann, D., Formolo, M., Tomasini, J., Krastel, S., Kaste, S., 2011. An interdisciplinary investigation of recent submarine mass transport deposit at the continental margin off Uruguay. *Geochemistry Geophysics Geosystem* 12, Q08009.
- Hensen, C., Zabel, M., Pfeifer, K., Schwenk, T., Kasten, S., Riedinger, N., Schulz, H.D., Boetius, A., 2003. Control of sulfate pore-water profiles by sedimentary events and the significance of anaerobic oxidation of methane for burial of sulfur in marine sediments. *Geochim. Cosmochim. Acta* 67, 2631–2647
- Hinrichs, K.U., Boetius, A.B., 2002. The anaerobic oxidation of methane: new insights in microbial ecology and biogeochemistry. In *Ocean Margin Systems*. Wefer, G., Billet, D., Hebbeln, D., Jørgensen, B.B., Schlüter, M., and van Weering, T. (Eds). Heidelberg: Springer-Verlag, pp. 457–477.
- Heinrich, S.M., Reeburgh, W.S., 1987. Anaerobic mineralization of marine sediment organic matter: rates and the role of anaerobic processes in the oceanic carbon economy. *Journal of Geomicrobiology* 5, 191-237.
- Hiruta, A., Snyder, G. T., Tomaru, H., Matsumoto, R., 2009. Geochemical constraints for the formation and dissociation of gas hydrate in an area of high methane flux, eastern margin of the Japan Sea. *Earth and Planetary Science Letter* 279, 326-339.
- Hovland, M., Curzi, P., 1989. Gas seepage and assumed mud diapirism in the Italian central Adriatic Sea. *Marine Petroleum Geology* 6, 161-169.
- Hovland, M., Talbot, M., Olausson, S., Aasberg, L., 1985. Recently formed methane-derived carbonates from the North Sea floor. In: Thomas, B.M. (Ed.) *Petroleum Geochemistry in Exploration of the Norwegian Shelf*. Norwegian Petroleum Soc., Graham & Trotman, 263-266.
- Hyndman, R.D., Spence, G.D., 1992. A Seismic Study of Methane Hydrate Marine Bottom Simulating Reflectors. *Journal of Geophysical Research* 97, 6683-6698.
- Iversen, N., Jørgensen, B.B., 1993. Diffusion coefficients of sulfate and methane in marine sediments: Influence of porosity. *Geochimica et Cosmochimica Acta* 57, 571–578.

- Iversen, N., Jørgensen, B. B., 1985. Anaerobic methane oxidation rates at the sulfate-methane transition in marine sediment from Kattegat and Skagerrak (Denmark). *Limnology and Oceanography* 30, 944-955.
- Jørgensen, B., 1977. The sulfur cycle of a coastal marine sediment (Limfjorden, Denmark). *Limnology and Oceanography* 22, 814-832.
- Jørgensen, B., 1982. Mineralization of organic matter in the sea bed—the role of sulphate reduction. *Nature* 296, 643-645.
- Judd, A.G., Hovland, M., 2007. *Submarine Fluid Flow, the Impact on Geology, Biology, and the Marine Environment*. Cambridge University Press. 475pp.
- Kasten, S., Jørgensen, B.B., 2000. Sulfate Reduction in Marine Sediments. In: Schulz, H.D and Zabel, M. (Eds.) *Marine Geochemistry*. pp263-275.
- Kastner, M., Claypool, G., Robertson, G., 2008. Geochemical constraints on the origin of the pore fluids and gas hydrate distribution at Atwater Valley and Keathly Canyon, northern Gulf of Mexico. *Marine Petroleum Geology* 25, 86-872.
- Knittel, K., Boetius, A., 2009. Anaerobic oxidation of methane: progress with as unknown process. *Annual Review of Microbiology* 63, 311-334.
- Krüger, M., Meyerdierks, A., Glöckner, F.O., Amann, R., Widdel, F., Kube, M., Reinhardt, R., Kahnt, J., Böcher, R., Thauer, R.K., 2003. A conspicuous nickel protein in microbial mats that oxidise methane anaerobically. *Nature* 426, 878–881.
- Kvenvolden, K., 1993. Gas hydrates-Geological perspective and global change. *Review of Geophysics* 31, 173–187.
- Koroleff, F., 1976. Determination of  $\text{NH}_4\text{-N}$ . In: Grasshoff, K (Ed.) *Method of seawater analysis*, Verlag Chemie. Weinheim, pp 126-133
- Kristensen, E., 2000. Organic matter diagenesis at the oxic/anoxic interface in coastal marine sediments, with emphasis on the role of burrowing animals. *Hydrobiologia* 426, 1-24.
- Lashof, D.A., Ahuja, D.R., 1990. Relative contributions of greenhouse gas emissions to global warming. *Nature* 344, 529-531.
- Li, Y.H., Gregory, S. 1974. Diffusion of ions in sea water and in deep sea sediments. *Geochimica et Cosmochimica Acta* 38, 703-714.
- Madigan, M., Martinko, J., Parker, J., 2000. *Brock Biology of Microorganisms*, Prentice-Hall, New Jersey, 991p.
- Mackin, J.E., Aller, R.C., 1984. Ammonium adsorption in marine sediments. *Limnology and Oceanography* 29, 250-257.
- Martens, C.S., Berner, R., 1974. Methane production in the interstitial waters of sulfate-depleted marine sediments. *Science* 185, 1167-1169.



- Mazumdar, A., Dewangan, P., João, H.M., Peketi, A., Khosla, V.R., Kocherla, M., Badesab, F. K., Joshi, R. Roxanne, P., Ramamurty, P.B.S., Karisiddaiah, M. Patil, D.J., Dayal, A.M, Hawkesworth C.J., Avanzinelli, R., Ramprasad, T., 2009. Evidence of paleo-cold seep activity from the Bay of Bengal, offshore India. *Geochemistry Geophysics Geosystem* 10, 1-15.
- Mazumdar A, Joshi R. K., Peketi, A., Naik B.G, 2011a. Variation in Carbon Stable Isotope Ratios of Organic Matter in Bay of Bengal during the Last Glacial Episode, Goldschmidt conference, Prague, Abstracts, p.1435.
- Mazumdar, A., Joshi, R.K., Peketi, A., Kocherla, M., 2011b. Occurrence of faecal pellet-filled simple and composite burrows in cold seep carbonates: A glimpse of a complex benthic ecosystem. *Marine Geology* 289, 117-121.
- Megonigal, J.P., Hines, M.E., Visscher, P.T., 2003. Anaerobic Metabolism: Linkages to Trace Gases and Aerobic Processes. In: Holland, H.D., Turekian, K.K. (Eds.), *Treatise on Geochemistry* 8, Biogeochemistry. Elsevier Pergamon. 317-424.
- Niewohner, C., Hensen, C., Kasten, S., Zabel., M., Schulz. H.D., 1998. Deep sulfate reduction completely mediated by anaerobic methane oxidation in sediments of the upwelling area off Namibia. *Geochimica et Cosmochimica Acta* 62, 455-464.
- NIO Technical Report, 2005. Geoscientific Investigations of Shallow Sediments in Krishna Godavari, East Coast. National Gas Hydrate Research Program report (NIO/TR-12-2003), Unpublished, p. 84.
- Orphan, V.J., House, C.H., Hinrichs, K.-U., McKeegan, K.D., DeLong, E.F., 2001. Methane consuming Archaea revealed by directly coupled isotopic and phylogenetic analysis. *Science* 293, 484-487.
- Powell, C.M., Roots, S.R., Veevers, J.J., 1988. Pre-breakup continental extension in east Gondwanaland and the early opening of the eastern Indian Ocean. *Tectonophysics* 155, 261-283.
- Paull, C.K., Ussler III, W., 2001. History and significance of gas sampling during DSDP and ODP drilling associated with gas hydrates. In: Paull, C.K., Dillon, W.P. (Eds.), *Natural Gas Hydrates: Occurrence, Distribution and Detection*. American Geophysical Union, Washington, DC, pp. 53-65.
- Prabhakar, K.N., Zutshi, P.L., 1993. Evolution of southern part of Indian east coast basins. *Journal of Geological Society of India* 41, 215-230.
- Ramana, M.V., Ramprasad, T., Kamesh Raju, K.A., Desa M., 2007. Occurrence of gas hydrates along the continental margins of India, particularly the Krishna-Godavari offshore basin. *International Journal of Environmental Studies* 64, 675-693.

- Ramana, M.V., Nair, R.R., Sarma, K.V.L.N.S., Ramprasad, T., Krishna, K.S., Subrahmanyam, V., D’Cruz, M., Subrahmanyam, C., Paul, J., Subrahmanyam, A.S., Sekhar, D.V.C., 1994. Mesozoic anomalies in the Bay of Bengal. *Earth and Planetary Science Letter* 121, 469-475.
- Ramesh, R., Subramanian, V., 1988. Temporal, spatial and size variation in the sediment transport in the Krishna River basin, India. *Journal of Hydrology* 98, 53-65.
- Ramprasad, T., Dewangan, P., Ramana, M.V., Mazumdar, A., Karisiddaiah, S.M., Ramya, E.R., Sriram, G., 2011. Evidence of slumping/sliding in Krishna-Godavari offshore basin due to gas/ fluid movements. *Marine petroleum Geology* 28, 1806-1816.
- Rao, G.N., 2001. Sedimentation, stratigraphy, and petroleum potential of Krishna-Godavari basin, east coast of India. *AAPG Bull.* 85, 1623-1643.
- Rao, G.N., Mani, K.S., 1993. A study on generation of abnormal pressures in Krishna-Godavari basin. *Indian Journal of Petroleum Geology* 2, 20-30.
- Reeburgh, W.S., 2007. Ocean methane biogeochemistry. *Chemical Review* 107, 486-513.
- Riedel, M., Collett, T.S., Kumar, P., Sathe, A.V., Cook, A., 2010. Seismic imaging of a fractured gas hydrate system in the Krishna-Godavari Basin offshore India. *Marine Petroleum Geology* 27, 1476-1493.
- Rodriguez, N., Paull, C., Borowski, W., 2000. Zonation of Authigenic carbonates within Gas Hydrate-bearing sedimentary sections on the Blake ridge: Offshore southeastern north America. In: Paull, C.K., Matsumoto, R., Wallace, P.J., and Dillon, W.P. (Eds.), *Proceedings of the Ocean Drilling Program, Scientific Results*, 164, pp. 301.
- Scheller, S., Goenrich, M., Boecher, R., Thauer, R.K., Jaun, B., 2010. The key nickel enzyme of methanogenesis catalyses the anaerobic oxidation of methane. *Nature* 465, 606-608.
- Schulz, H.D., Zabel, M., 2000. *Marine Geochemistry*. Springer, Berlin, Heidelberg, New York, pp 455.
- Scotese, C.R., Gahagan, L.M., Larson, R.L., 1988. Plate tectonic reconstructions of the Cretaceous and Cenozoic ocean basins. *Tectonophysics* 155, 27-48.
- Schönheit, P., Keweloh, H., Thauer, R.K., 1981, Factor F<sub>420</sub> degradation in *Methanobacterium thermoautotrophicum* during exposure to oxygen. *FEMS Microbiology Letter* 12, 347-349.
- Schrum, H.N., Spivack, A.J., Kastner, M. and D’Hondt, S., 2009. Sulfate-reducing ammonium oxidation: A thermodynamically feasible metabolic pathway in subseafloor sediment. *Geology* 37, 939-942.
- Schmidt, M., Hensen, C., Mörz, T., Müller, C., Grevemeyer, I., Wallmann, K., Mau, S. and Kaul, N., 2005. Methane hydrate accumulation in "Mound 11" mud volcano, Costa Rica forearc. *Marine Geology* 216, 83-100.
- Suess, E., Torres, M.E., Bohrmann, G., Collier, R.W., Greinert, J., Linke, P., Rehder, G., Trehu, A., Wallmann, K., Winckler, G., Zuleger, E., 1999. Gas hydrate destabilization: enhanced

- dewatering, benthic material turnover and large methane plumes at the Cascadia convergent margin. *Earth and Planetary Science Letter* 170, 1–15.
- Sloan, E.D., 1998. *Clathrate Hydrates of Natural Gases*. Marcel Dekker, Inc., New York, 641 pp.
- Solomon, E.A., Spivack, A., Kastner, M., Torres, M., Borole, D. V., Robertson, G., Das, H.C., 2008. Hydrogeochemical and structural controls on heterogeneous gas hydrate distribution in the K-G basin offshore, India. In: *Proceedings of the 6th International Conference on Gas Hydrates (ICGH 2008)*, Vancouver, British Columbia, Canada.
- Tomaru, H., Matsumoto, R., Coffin, R.B., Pohlman, J.W., Spence, G.D., 2007. Geochemical relation between hydrates and water venting in the seismic zone on the northern Cascadia continental margin offshore Vancouver Island, Canada. *Journal of Geochemical Exploration* 95, 40-47.
- Tréhu A.M., 2007. Preliminary results from in situ temperature measurements made during NGHP-01 (extended abstract), NGHP-01 post-cruise meeting, Noida, India.
- Tréude, T., Niggemann, J., Kallmeyer, J., Wintersteller, P., Schubert, C.J., Boetius, A., Jørgensen, B.B., 2005. Anaerobic oxidation of methane in the sulfate–methane transition along the Chilean continental margin. *Geochimica et Cosmochimica Acta* 69, 2767–2779.
- Ussler III, W., Paull, C.K., 2008. Rates of anaerobic oxidation of methane and authigenic carbonate mineralization in methane-rich deep-sea sediments inferred from models and geochemical profiles, *Earth and Planetary Science Letter* 266, 271-287.
- Valentine, D.L., Reeburgh, W.S., 2000. New perspectives on anaerobic methane oxidation. *Environmental Microbiology* 2, 477–484.
- Wallmann, K., Aloisi, G., Haeckel, M., Tishchenko, P., Pavlova, G Greinert, J., Kutterolf, S., Eisenhauer, A., 2008. Silicate weathering in anoxic marine sediments., *Geochimica et Cosmochimica Acta* 72, 3067–3090.
- Westrich, J.T., Berner, R.A., 1988. The effect of temperature on rates of sulfate reduction in marine sediments. *Journal of Geomicrobiol* 6, 99-117.
- Whiticar, M.J., 1999. Carbon and hydrogen isotope systematics of bacterial formation and oxidation of methane. *Chemical Geology* 161, 291–314.
- Whiticar, M.J., Faber, E., 1986. Methane oxidation in sediment and water column environments - Isotope evidence. *Organic Geochemistry* 10, 759-768.
- Zabel, M., Schulz, H.D., 2001. Importance of submarine landslides for non-steady state conditions in pore water system-lower Zaire (Congo) deep-sea fan. *Mar. Geol.* 176, 87-99.

## Figure and Table captions

**Figure 1.** Bathymetry map displaying core locations and fault lines. Stars represent the location of the cores collected onboard JOIDES Resolution (labelled as J) and white circles indicate the location of the cores collected onboard Marion Dufresne (labelled as M). The thick blue line represents the multi channel seismic line.

**Figure 2.** SBP data across different coring locations showing nature of layering and acoustic voids. A. Acoustic voids in upper layered sediments underlain by acoustic transparent masses with few internal reflectors. B. Onlap of MTDs against a mud mound. C. Finely layered sediments with growth faults. D. Layered sediments and underlying acoustically transparent mass. E. Acoustically transparent mass with fault. F. Multi channel seismic data displaying BSR and regional fault system.

**Figure 3.** A and B. zoom-outs of SBP data across MD161-12 and 13 showing growth fault, acoustic voids and mass transport deposits (MTD). C and D. SBP data across MD161-1 and 2 displaying MTD and faults.

**Figure 4.** Variation in thickness of the Holocene drupe sediment with water depth derived from the regional SBP profile.

**Figure 5.** Age-depth models for MD161-1, 7, 8, 11 and 13. The dotted lines show the abrupt change in sedimentation rates. The age data of MD161-8 is from Mazumdar et al., (2009).

**Figure 6** A-J. Sulfate, alkalinity and methane concentration profiles. Sulfate and alkalinity concentrations are in milimolar (mM) and methane concentrations are in micromolar ( $\mu\text{M}$ ).

**Figure 7.** Chloride concentration (milimolar) profiles.

**Figure 8.** Carbon isotope ratios of headspace  $\text{CO}_2$  and  $\text{CH}_4$  gases.

**Figure 9.** Cross plot of  $\text{C1/C2+C3}$  and carbon isotope ratios of headspace gases.

**Figure 10.** Ammonium concentration variation with depth below seafloor.

**Figure 11.** TOC concentration variation with depth below seafloor.

**Figure 12.**  $\delta^{13}\text{C}_{\text{TIC}}$  and  $\delta^{18}\text{O}_{\text{TIC}}$  profiles of MD161-8.

**Table-1:** Concentrations and isotope ratios of various dissolved components in the porewaters and head space gases. nd= not detectable.

**Supplementary Table-1:** Total organic carbon concentrations.

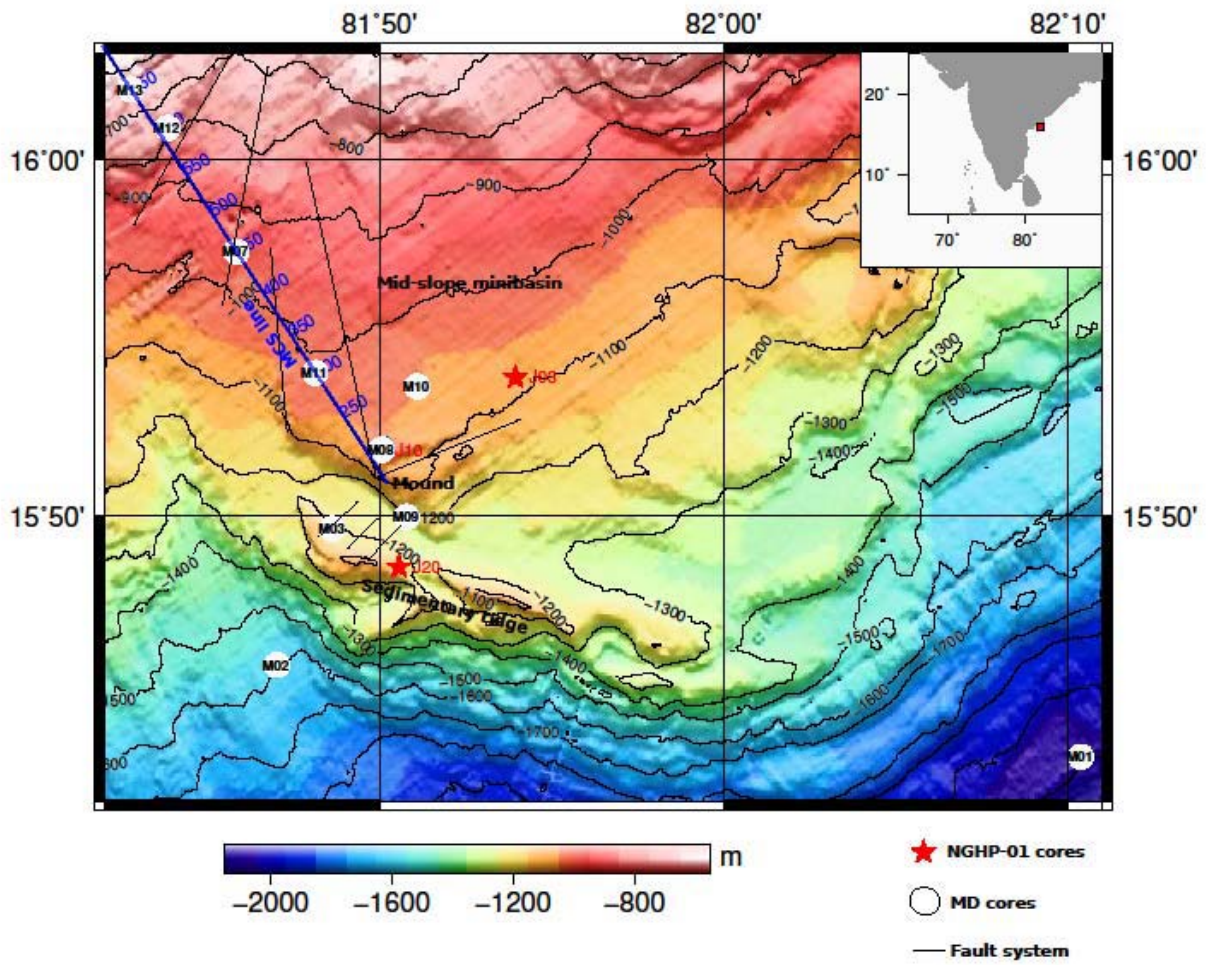


Figure 1

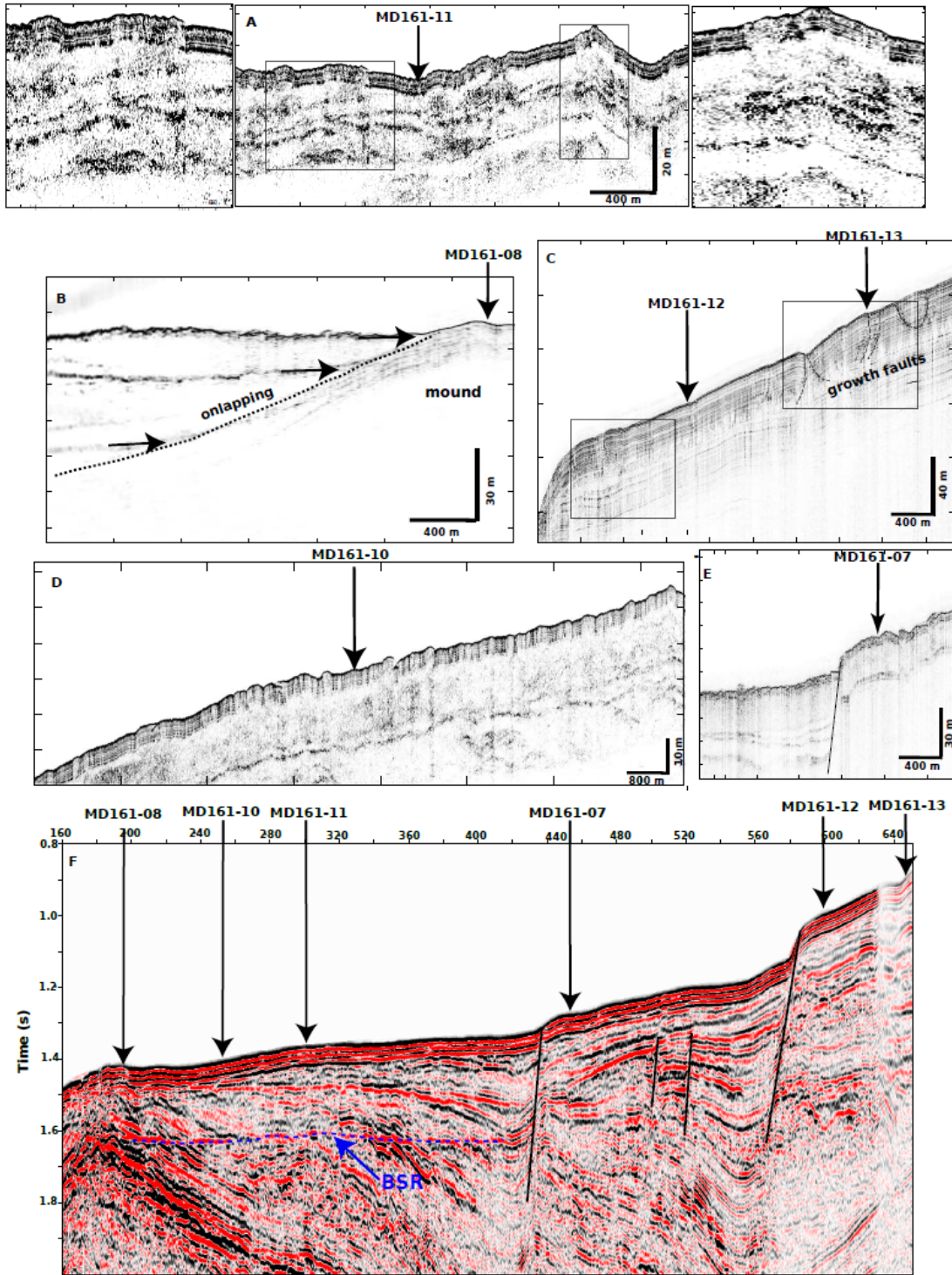


Figure :2



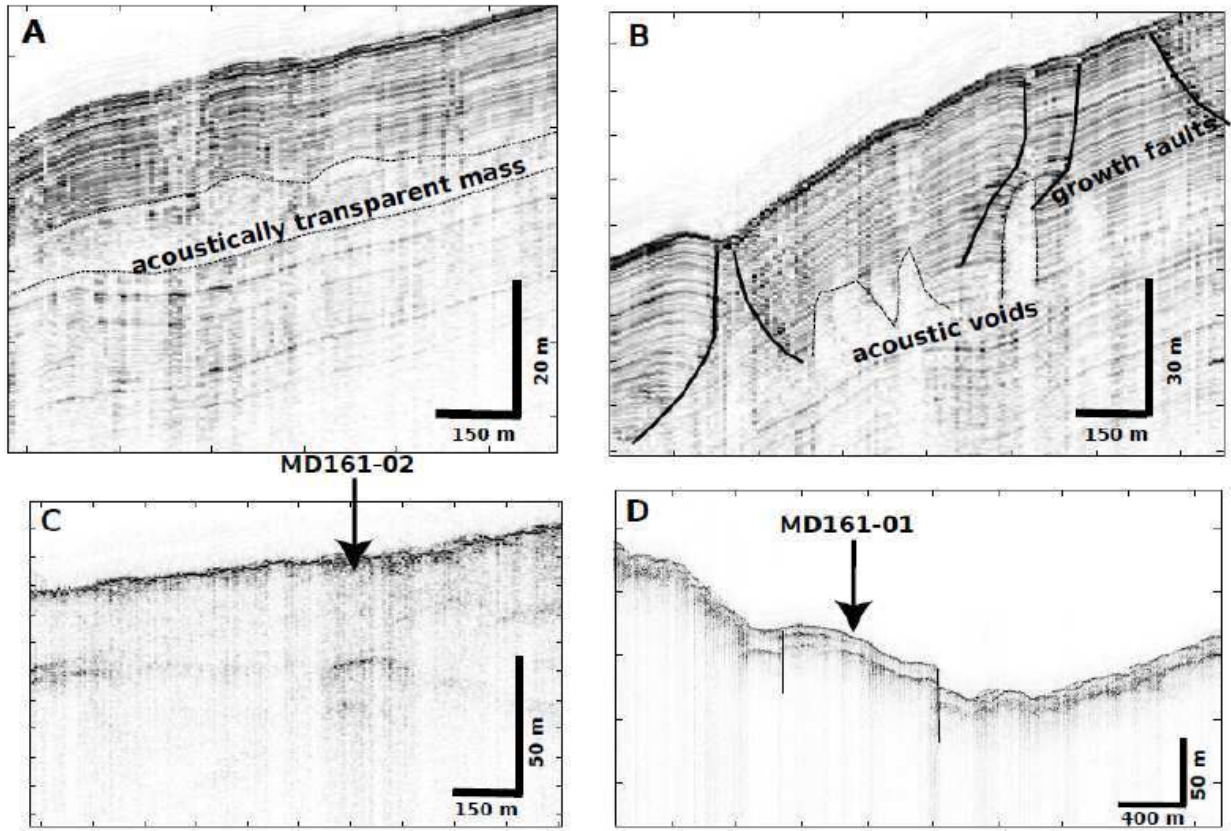
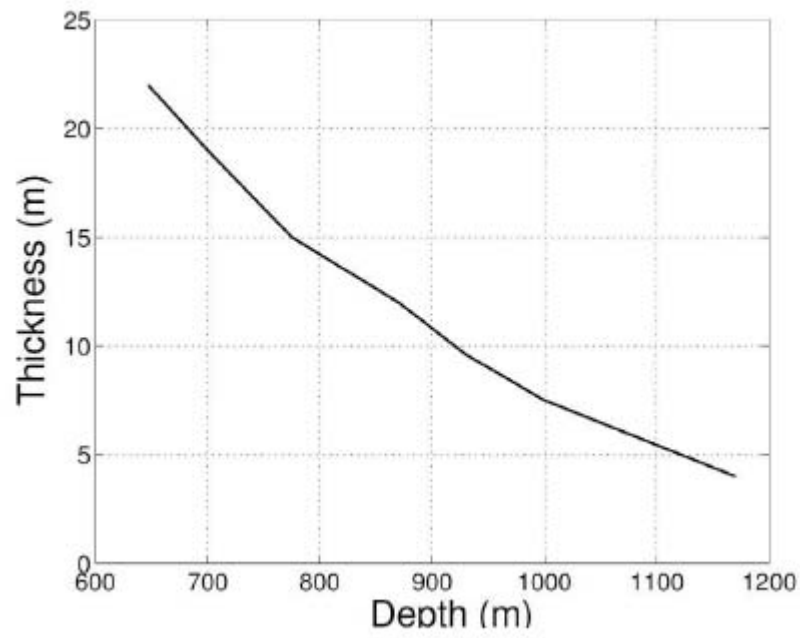


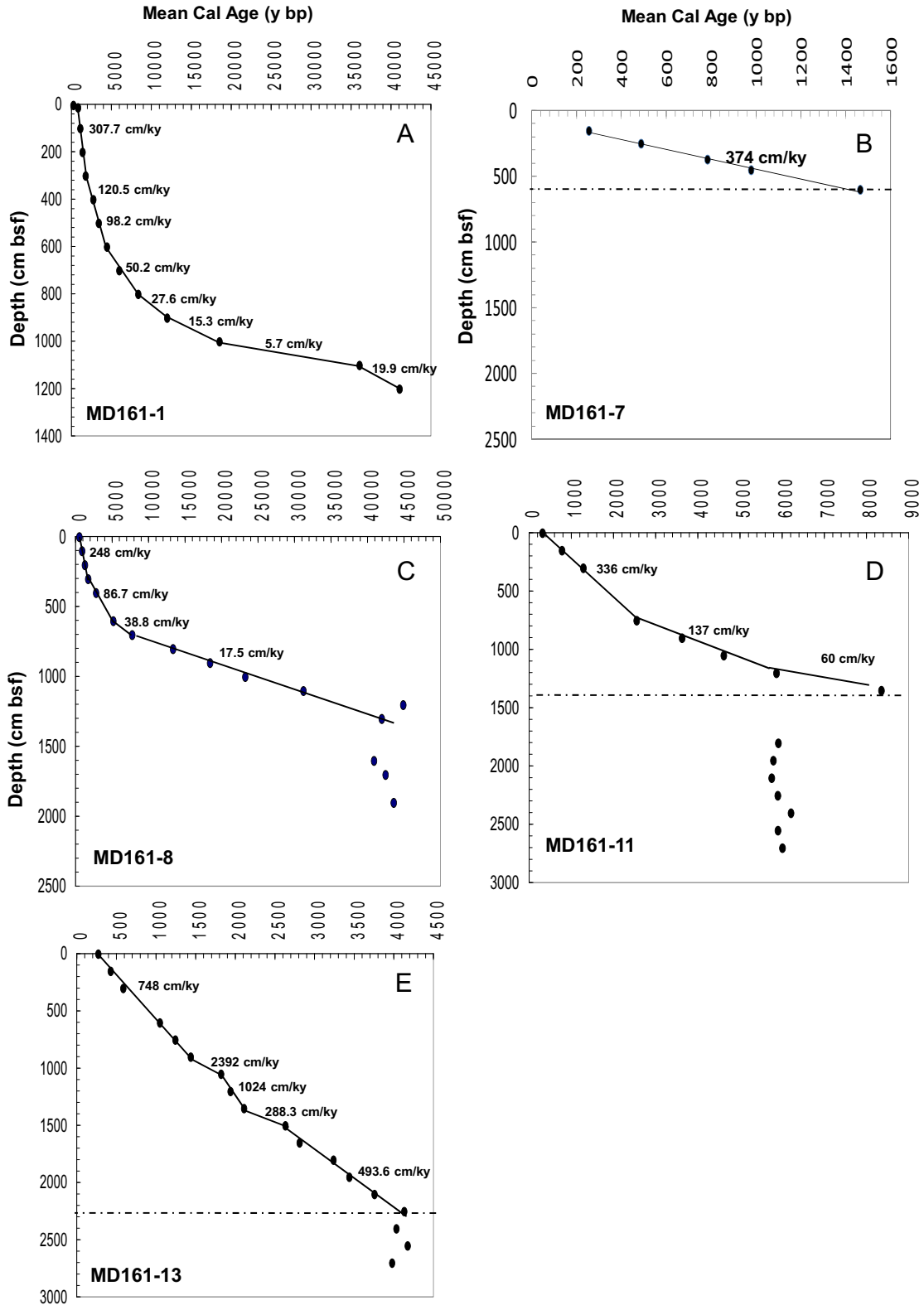
Figure:3



**Figure-4**



Figure 5



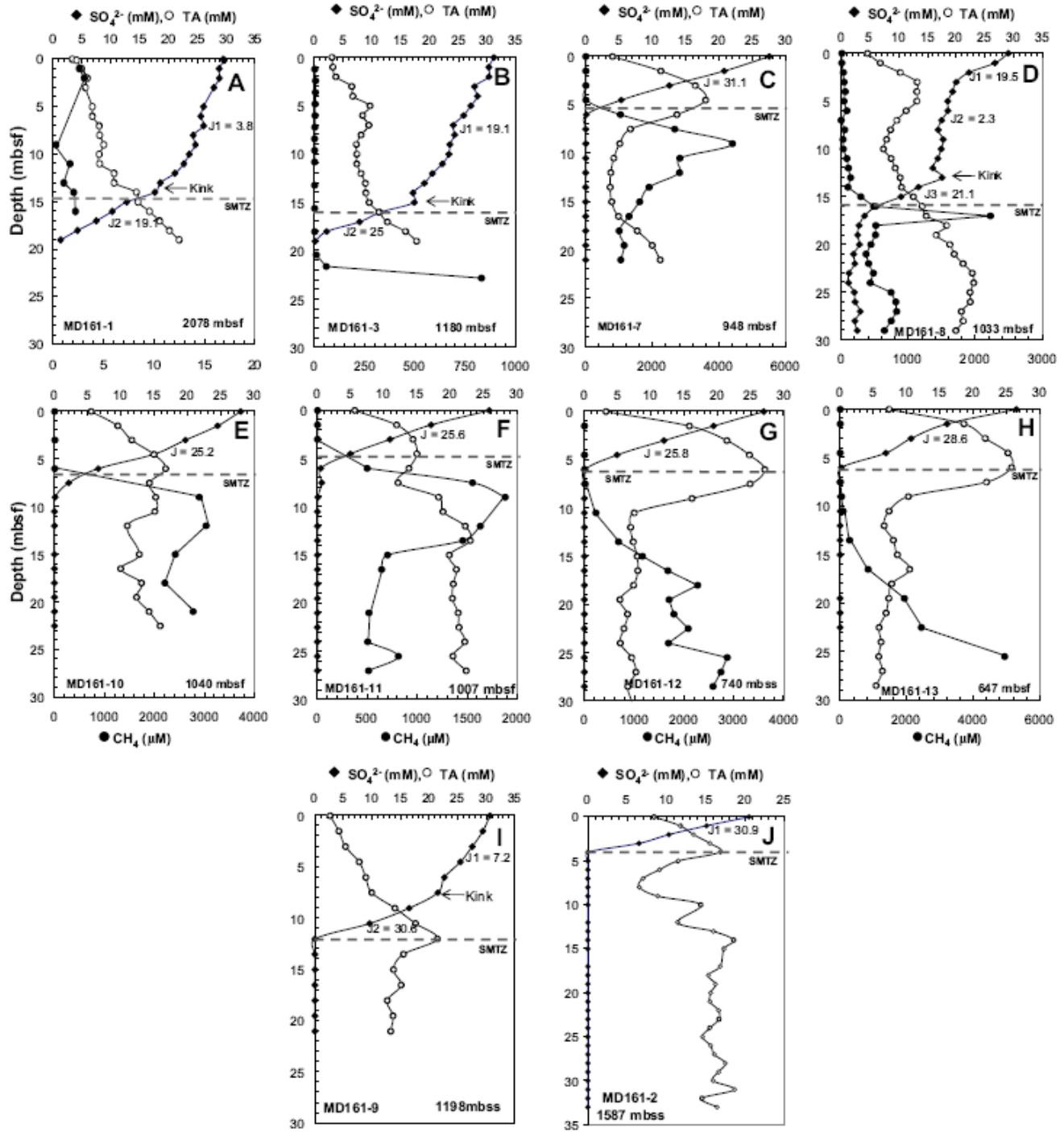


Figure6A-B

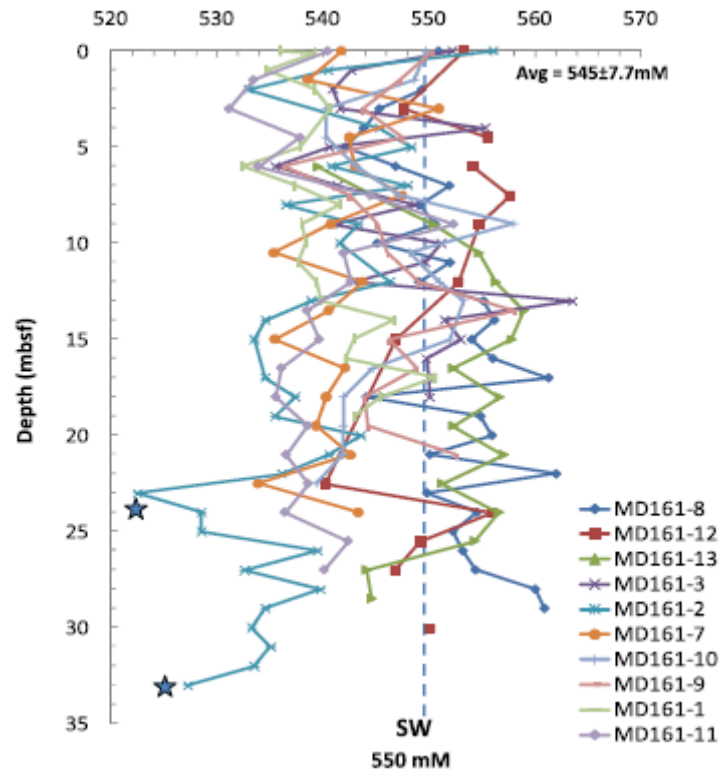


Figure7

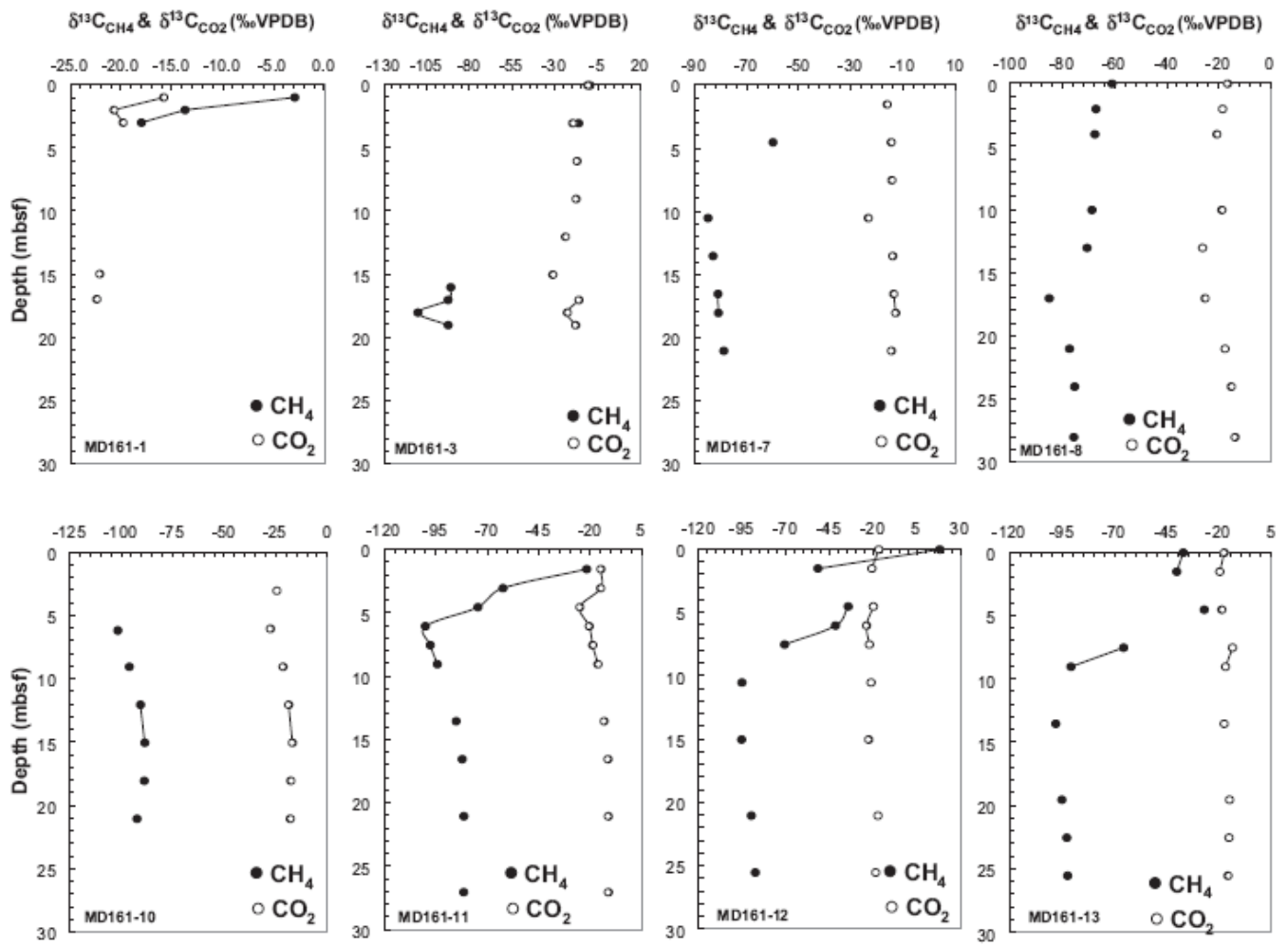
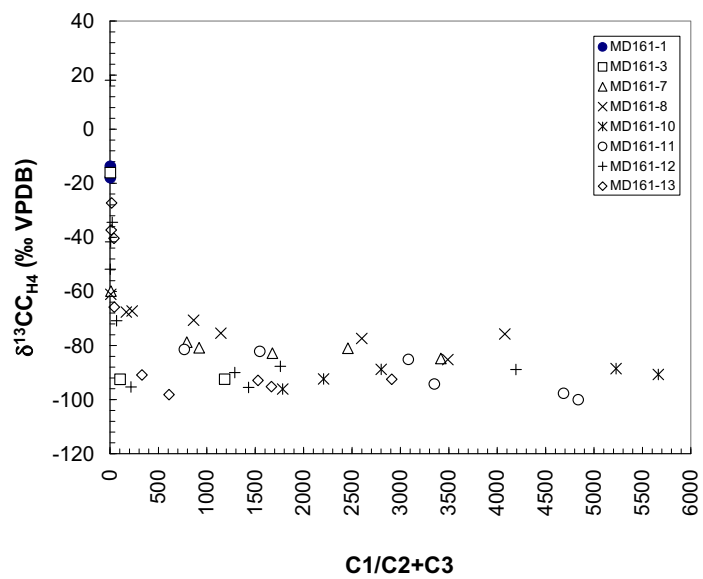


Figure8

Figure9



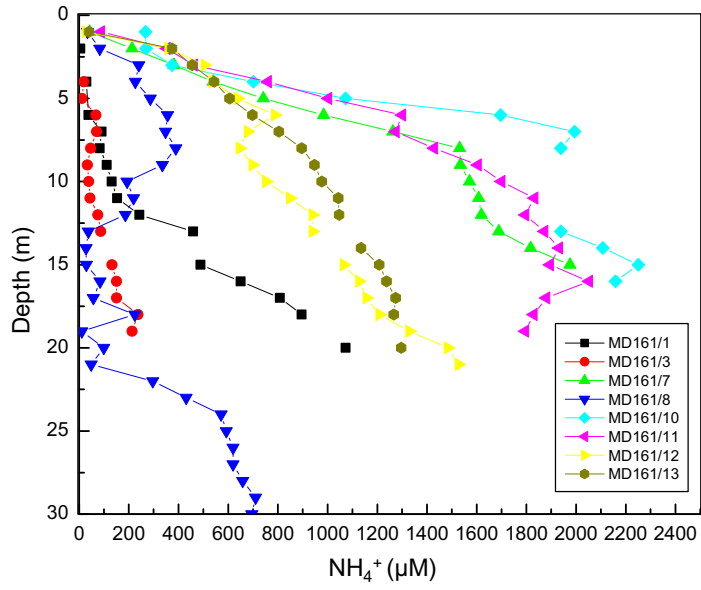


Figure10

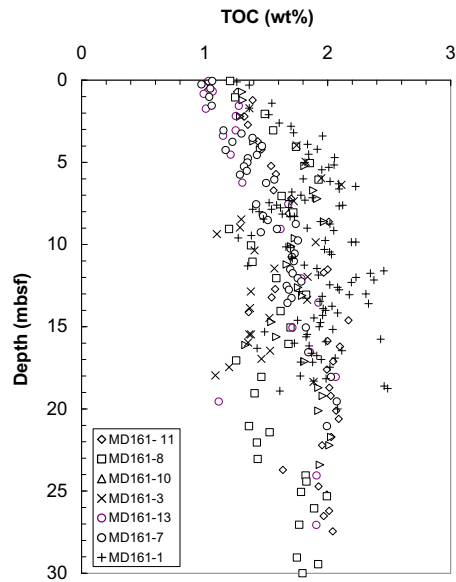


Figure 11

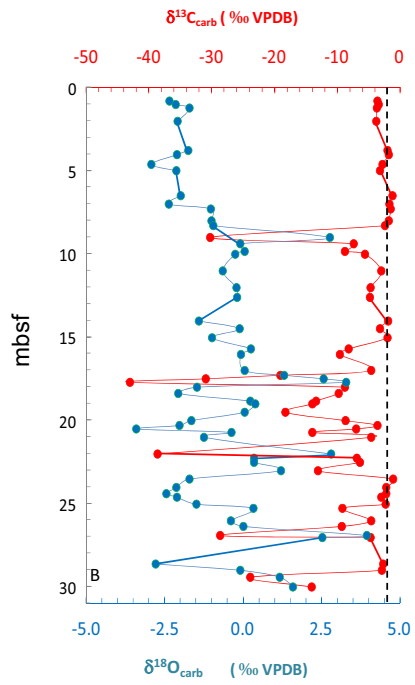


Figure 12

Table-1

## MD161-1

Depth (mbsf)	SO <sub>4</sub> (mM)	TA (mM)	NH <sub>4</sub> (μM)	Alk (mM)	CH <sub>4</sub> (μM)	C1/(C2+C3)	δ <sup>13</sup> C CH <sub>4</sub> (‰ VPDB)	δ <sup>13</sup> C CO <sub>2</sub> (‰ VPDB)	CI (mM)
0.05	29.5	3.4		3.4					536.0
0.15	29.7	4.1		4.1			-2.9	-15.8	539.3
1.03	28.8	5.0	4.9	5.0	2.6		-13.7	-20.7	534.8
2.03	28.8	6.0		6.0	3.1		-18.0	-19.8	539.2
3.03	27.9	5.6	29.4	5.6					540.7
5.03	26.1	6.8	37.9	6.8					537.9
6.03	25.6	6.8	90.6	6.8					532.5
7.03	26.1	8.0	83.2	8.0					537.4
8.03	24.3	8.1	111.4	8.1					541.6
9.03	24.7	8.8	131.0	8.8	0.3				538.0
10.03	23.6	8.0	153.0	8.0					538.4
11.03	22.7	8.1	242.4	8.1	1.7				537.7
12.03	21.2	10.6	459.0	10.6					539.4
13.03	18.6	10.6		10.6	1.1				539.8
14.03	17.7	14.5	488.4	14.5	2.1			-22.1	546.7
15.03	12.8	14.8	649.9	14.8					543.0
16.03	10.3	16.7	807.8	16.7	2.3			-22.4	542.2
17.03	7.5	18.5	896.0	18.5					550.6
18.03	4.3	20.2		20.2					545.4
19.03	1.4	21.9	1072.2	21.9					543.1

## MD161-2

Depth (mbsf)	SO <sub>4</sub> (mM)	TA (mM)	NH <sub>4</sub> (μM)	Alk (mM)	CH <sub>4</sub> (μM)	C1/(C2+C3)	δ <sup>13</sup> C CH <sub>4</sub> (‰ VPDB)	δ <sup>13</sup> C CO <sub>2</sub> (‰ VPDB)	CI (mM)
0.05	20.5	8.4		8.4					556.0
1.055	15.1	11.8		11.8					540.5
2.055	10.3	13.5		13.5					532.9
3.055	6.5	15.5		15.5					568.7
4.055	nd	16.9		16.9					545.4
5.055	nd	11.5		11.5					548.3
6.055	nd	9.1		9.1					540.8
7.055	nd	7.0		7.0					548.0
8.055	nd	6.6		6.6					536.5
9.055	nd	8.9		8.9					543.3
10.055	nd	14.4		14.4					541.6
12.055	nd	11.4		11.4					546.3
13.055	nd	16.0		16.0					538.9
14.055	nd	18.6		18.6					534.5
15.055	nd	17.4		17.4					533.5
17.055	nd	16.9		16.9					534.6
18.055	nd	15.3		15.3					537.4
19.055	nd	16.3		16.3					535.5
20.055	nd	15.6		15.6					543.6
21.055	nd	15.5		15.5					540.6
22.055	nd	16.7		16.7					536.1
23.055	nd	16.7		16.7					522.5
24.055	nd	15.5		15.5					528.5



25.055	nd	14.6		14.6					528.5
26.055	nd	15.6		15.6					539.5
27.055	nd	16.1		16.1					532.6
28.055	nd	17.5		17.5					539.7
29.055	nd	16.7		16.7					534.6
30.055	nd	16.0		16.0					533.3
31.055	nd	18.7		18.7					535.1
32.055	nd	14.5		14.5					533.5
33.055	nd	16.5		16.5					527.2

### MD161-3

Depth (mbsf)	SO <sub>4</sub> (mM)	TA (mM)	NH <sub>4</sub> (μM)	Alk (mM)	CH <sub>4</sub> (μM)	C1/(C2+C3)	δ <sup>13</sup> C CH <sub>4</sub> (‰ VPDB)	δ <sup>13</sup> C CO <sub>2</sub> (‰ VPDB)	Cl (mM)
0.05	31.2	3.0		3.0			-9.5	-10.9	552.2
1.055	30.3	3.2		3.2	0.9	3.5			542.7
2.055	30.3	3.7		3.7	4.8	1.8			541.0
3.055	27.8	6.5	18.9	6.5	3.9	2.7	-16.1	-19.6	541.7
4.055	28.3	6.7	11.6	6.7	2.5				555.3
5.055	27.2	9.6	67.9	9.6	2.4	4.0			540.6
6.055	25.9	8.3	70.3	8.3	1.3	3.4		-17.1	535.6
7.055	24.1	9.4	46.5	9.4	0.1	6.0			541.4
8.055	24.4	8.1	33.0	8.1	0.2				548.7
9.055	23.5	7.3	39.2	7.3	0.3			-17.5	540.9
10.055	23.4	7.3	44.1	7.3					551.2
11.055	22.2	7.3	75.9	7.3	0.2				549.6
12.055	20.5	8.1	86.9	8.1		9.5		-23.8	542.9
13.055	19.1	8.8		8.8	0.2				563.5
14.055	17.1	8.9	132.2	8.9					551.5
15.055	17.3	9.5	150.6	9.5	0.5	3.1		-31.2	553.0
16.055	11.5	11.2	150.6	11.2			-90.9		549.8
17.055	7.8	12.7	237.5	12.7	8.3	103.4	-92.5	-15.9	550.0
18.055	2.1	15.8	213.0	15.8	58.1		-110.2	-22.7	550.1
19.055	0.1	17.7		17.7	828.9	1184.2	-92.5	-17.8	

### MD161-7

Depth (mbsf)	SO <sub>4</sub> (mM)	TA (mM)	NH <sub>4</sub> (μM)	Alk (mM)	CH <sub>4</sub> (μM)	C1/(C2+C3)	δ <sup>13</sup> C CH <sub>4</sub> (‰ VPDB)	δ <sup>13</sup> C CO <sub>2</sub> (‰ VPDB)	Cl (mM)
0.05	27.5	4.0	42.2	4.0	2.2	4.1			541.7
1.55	20.7	11.3	213.0	11.3	3.5	8.7		-16.2	538.6
3.055	12.5	16.4	381.9	16.4	3.6	4.3			550.9
4.55	5.3	18.0	539.8	18.0	5.3	8.2	-59.9	-14.6	542.5
6.055	0.1	13.7	741.7	13.7	1038.5				543.0
7.55	nd	6.7	984.1	6.7	2662.1	3393.3		-14.4	547.4
9.055	nd	5.1	1263.2	5.1	4390.9	1367.1			540.8
10.55	nd	4.2	1531.2	4.2	2817.3	3417.0	-84.8	-23.4	543.7
12.055	nd	3.8	1534.9	3.8	2807.8	8813.8			540.6
13.55	nd	3.7	1571.6	3.7	1897.6	1676.9	-82.9	-14.0	542.1
15.055	nd	3.9	1608.3	3.9	1614.1	1502.2			540.3
16.55	nd	4.9	1619.3	4.9	1295.0	2457.2	-81.0	-13.6	539.4
18.055	nd	7.7	1689.1	7.7	1002.2	920.8	-80.8	-12.9	542.6
19.55	nd	10.0	1817.6	10.0	1148.9	1133.2			533.9
21.055	nd	11.2	1975.5	11.2	1048.1	791.8	-78.7	-14.5	543.3

**MD161-8**

Depth (mbsf)	SO <sub>4</sub> (mM)	TA (mM)	NH <sub>4</sub> (μM)	Alk (mM)	CH <sub>4</sub> (μM)	C1/(C2+C3)	δ <sup>13</sup> C CH <sub>4</sub> (‰ VPDB)	δ <sup>13</sup> C CO <sub>2</sub> (‰ VPDB)	Cl (mM)
0.05	29.1	4.6	33.7	4.6	12.1	7.6	-61.1	-16.6	550.9
1.055	26.7	6.8	83.2	6.8	9.8	47.4			564.0
2.055	22.2	10.3	239.9	10.3	33.2	227.4	-67.2	-18.6	549.3
3.055	20.0	13.2	226.4	13.2	43.4	366.0			545.3
4.055	19.4	13.2	286.4	13.2	61.5	167.1	-67.6	-20.8	543.9
5.055	18.5	13.2	356.2	13.2	40.6	192.7			542.1
6.055	18.6	11.3	347.6	11.3	86.3	224.0			546.9
7.055	17.5	9.7	389.2	9.7	1.0				551.9
8.055	16.9	8.6	335.4	8.6	52.9				549.1
9.055	17.7	7.9	193.4	7.9	28.6				550.6
10.055	17.4	7.4	219.1	7.4	31.7		-68.8	-18.9	545.1
11.055	16.8	8.7	186.0	8.7	85.4	709.2			552.0
12.055	16.0	9.4	37.3	9.4	108.8				549.0
13.055	17.6	10.3	28.2	10.3	141.5	863.4	-70.7	-26.3	555.1
14.055	13.5	10.5	29.4	10.5	101.6	1293.5			556.2
15.055	10.4	12.6	84.5	12.6	292.7	1090.1			554.0
16.055	6.2	14.1	57.5	14.1	484.4	2376.3			556.0
17.055	4.1	14.8	224.0	14.8	2224.9	3489.1	-85.2	-25.3	561.3
18.055	3.1	18.3	11.0	18.3	516.8	3242.5			544.1
19.055	2.9	16.6	99.1	16.6	511.4	2898.1			554.9
20.055	3.2	18.9	49.0	18.9	443.9	3529.4			555.9
21.055	2.2	19.7	296.2	19.7	370.5	2600.4	-77.4	-17.7	550.1
22.055	2.4	21.2	430.8	21.2	409.4	1948.9			562.0
23.055	1.4	22.8	571.6	22.8	481.3	3422.8			549.8
24.055	1.3	23.1	592.4	23.1	433.5	1144.6	-75.4	-15.3	554.5
25.055	2.3	22.4	619.3	22.4	744.7	4104.0			552.3
26.055	2.4	22.5	619.3	22.5	815.3	3494.6			553.2
27.055	3.3	20.9	658.5	20.9	827.9	4064.9			554.4
28.055	2.4	21.2	709.9	21.2	747.0	4077.2	-75.7	-13.8	560.0
29.055	2.8	20.0	695.2	20.0	644.7	2896.9			560.9

**MD161-9**

Depth (mbsf)	SO <sub>4</sub> (mM)	TA (mM)	NH <sub>4</sub> (μM)	Alk (mM)	CH <sub>4</sub> (μM)	C1/(C2+C3)	δ <sup>13</sup> C CH <sub>4</sub> (‰ VPDB)	δ <sup>13</sup> C CO <sub>2</sub> (‰ VPDB)	Cl (mM)
0.05	30.7	2.65		2.7					550.4
1.55	29.4	4.2		4.2					547.3
3.055	27.5	5.4		5.4					543.8
4.55	25.5	7.8		7.8					547.5
6.055	22.7	8.9		8.9					536.3
7.55	21.5	10.0		10.0					542.5
9.055	16.5	14.0		14.0					545.1
10.55	9.6	17.6		17.6					546.1
12.055	nd	21.5		21.5					549.0
13.55	nd	15.5		15.5					558.1
15.055	nd	13.8		13.8					546.2
16.55	nd	15.1		15.1					548.9
18.055	nd	12.7		12.7					544.0
19.55	nd	13.7		13.7					544.2
21.055	nd	13.3		13.3					552.6

**MD161-10**

Depth (mbsf)	SO <sub>4</sub> (mM)	TA (mM)	NH <sub>4</sub> (μM)	Alk (mM)	CH <sub>4</sub> (μM)	C1/(C2+C3)	δ <sup>13</sup> C CH <sub>4</sub> (‰ VPDB)	δ <sup>13</sup> C CO <sub>2</sub> (‰ VPDB)	Cl (mM)
0.05	28.0	5.5	266.8	5.5	2.2	5.4			549.7
1.55	24.5	9.5	269.3	9.5					548.6
3.055	19.7	11.6	374.5	11.6	7.6	1.5		-24.5	540.3
4.55	14.9	15.0	701.3	15.0					540.2
6.055	6.6	16.7	1072.2	16.7	5.8	6.6		-27.6	543.1
7.55	2.1	14.3	1696.5	14.3					547.1
9.055	0.1	15.2	1993.9	15.2	2899.1	1783.7	-96.1	-21.5	557.9
10.55	nd	15.1	1938.8	15.1					548.1
12.055	nd	10.9	1450.4	10.9	3034.1	5664.2	-90.7	-18.8	551.0
15.055	nd	12.7	1175.0	12.7	2419.4	5228.6	-88.6	-17.0	552.0
16.55	nd	9.9	1468.8	9.9					544.7
18.055	nd	13.1	1938.8	13.1	2209.0	2800.9	-88.8	-17.8	541.9
19.55	nd	12.3	2107.7	12.3					541.9
21.055	nd	14.2	2250.9	14.2	2775.9	2206.6	-92.4	-18.0	541.8
22.553	nd	15.9	2159.1	15.9					539.4

**MD161-11**

Depth (mbsf)	SO <sub>4</sub> (mM)	TA (mM)	NH <sub>4</sub> (μM)	Alk (mM)	CH <sub>4</sub> (μM)	C1/(C2+C3)	δ <sup>13</sup> C CH <sub>4</sub> (‰ VPDB)	δ <sup>13</sup> C CO <sub>2</sub> (‰ VPDB)	Cl (mM)
0.05	25.8	5.6	88.1	5.6	1.2	10.1			540.5
1.55	17.1	11.9	352.5	11.9	0.7		-21.8	-14.9	533.5
3.055	10.9	14.4	462.7	14.4	0.6		-62.4	-15.1	531.2
4.55	4.9	15.0	760.1	15.0			-74.6	-25.1	537.9
6.055	0.5	13.8	1002.4	13.8	497.5	4837.2	-100.1	-20.6	533.9
7.55	0.6	12.1	1299.9	12.1	1552.8	4685.8	-97.7	-18.9	544.5
9.055	0.1	18.2	1274.2	18.2	1879.4	3351.0	-94.3	-16.4	552.3
10.55	nd	18.9	1428.4	18.9					541.9
12.055	nd	22.2	1604.7	22.2	1630.5	1707.3			542.6
13.55	nd	23.0	1700.1	23.0	1454.8	3082.6	-85.2	-13.3	538.5
15.055	nd	19.8	1832.3	19.8	701.1	2001.3			539.6
16.55	nd	20.9	1795.6	20.9	642.4	1546.7	-82.2	-11.5	536.1
18.055	nd	20.4	1872.7	20.4					535.6
19.55	nd	20.3	1931.5	20.3					538.6
21.055	nd	21.1	1894.7	21.1	515.9		-81.4	-11.3	536.5
22.553	nd	21.3	2052.6	21.3					538.6
24.055	nd	22.1	1880.7	22.1	503.0	595.0			536.4
25.55	nd	20.3	1829.3	20.3	809.8	698.0			542.4
27.055	nd	22.3	1795.0	22.3	512.6	767.1	-81.5	-11.3	540.1

**MD161-12**

Depth (mbsf)	SO <sub>4</sub> (mM)	TA (mM)	NH <sub>4</sub> (μM)	Alk (mM)	CH <sub>4</sub> (μM)	C1/(C2+C3)	δ <sup>13</sup> C CH <sub>4</sub> (‰ VPDB)	δ <sup>13</sup> C CO <sub>2</sub> (‰ VPDB)	Cl (mM)
0.05	27.0	3.3	26.9	3.3		4.0	18.1	-16.9	553.2
1.55	19.4	15.8	358.6	15.8	2.2	3.5	-51.8	-20.8	
3.055	12.0	21.5	505.5	21.5					547.6
4.55	4.9	24.9	537.3	24.9	2.6	22.6	-34.4	-20.0	550.6
6.055	0.1	27.2	638.9	27.2	4.2	5.2	-41.7	-23.9	554.1
7.55	nd	25.0	788.2	25.0	16.0	67.6	-70.8	-22.2	557.6
9.055	nd	16.2	679.3	16.2					554.8

10.55	nd	7.5	646.3	7.5	231.2	216.5	-95.3	-21.3	
12.055	nd	7.0	697.7	7.0					552.8
13.55	nd	7.4	752.8	7.4	684.5	907.1			
15.055	nd	8.0	848.2	8.0	1166.8	1431.0	-95.5	-22.7	546.8
16.55	nd	8.1	940.0	8.1	1675.2	1781.3			
18.055	nd	7.4	940.0	7.4	2273.0	1312.9			
19.55	nd	5.4		5.4	1700.7	1478.2			
21.055	nd	6.5	1064.9	6.5	1796.1	1288.1	-90.0	-17.4	
22.55	nd	6.0	1127.3	6.0	2084.8	1492.0			540.2
24.055	nd	5.4	1156.7	5.4	1686.5	422.7			556.0
25.55	nd	7.1	1208.1	7.1	2866.1	1759.7	-87.7	-18.6	549.2
27.055	nd	7.8	1329.3	7.8	2741.8	3199.3			546.8
28.55	nd	6.6	1483.5	6.6	2581.9	1240.3			573.8
30.055	nd	7.1	1527.5	7.1		4193.1	-88.9	-18.8	550.1

### MD161-13

Depth (mbsf)	SO <sub>4</sub> (mM)	TA (mM)	NH <sub>4</sub> (μM)	Alk (mM)	CH <sub>4</sub> (μM)	C1/(C2+C3)	δ <sup>13</sup> C CH <sub>4</sub> (‰ VPDB)	δ <sup>13</sup> C CO <sub>2</sub> (‰ VPDB)	CI (mM)
0.05	26.5	7.4	40.4	7.4	4.3	10.8	-37.3	-17.7	544.1
1.55	16.1	18.6	374.5	18.6	3.6	40.9	-40.4	-19.8	556.4
3.055	10.7	21.8	455.3	21.8		14.1			548.6
4.55	6.9	25.2	543.5	25.2	1.8	16.4	-27.3	-18.9	547.7
6.055	0.2	25.8	605.9	25.8					539.6
7.55	nd	22.0	697.7	22.0	6.0	43.0	-65.8	-13.7	544.8
9.055	nd	10.3	804.2	10.3	44.8	328.6	-90.9	-17.1	550.4
10.55	nd	7.4	896.0	7.4	90.1	313.3			554.7
12.055	nd	6.6	947.4	6.6					556.3
13.55	nd	8.0	976.7	8.0	283.2	608.6	-98.2	-17.7	559.0
15.055	nd	8.6	1042.8	8.6					557.8
16.55	nd	10.5	1046.5	10.5	839.5	775.3			552.3
18.055	nd	7.8		7.8					556.7
19.55	nd	7.3	1134.6	7.3	1930.0	1666.8	-95.2	-15.2	552.3
21.055	nd	6.9	1208.1	6.9					557.1
22.55	nd	5.9	1237.5	5.9	2440.7	1527.9	-92.9	-15.4	551.3
24.055	nd	6.2	1274.2	6.2					556.6
25.55	nd	5.8	1266.8	5.8	4941.0	2910.8	-92.5	-15.9	554.3
27.055	nd	6.4		6.4					544.2
28.55	nd	5.4	1296.2	5.4					544.6

nd = not detectable

Supplementary Table-1

Depth (mbsf)	TOC (wt%) MD161-1	Depth (mbsf)	TOC (wt%) MD161-3	Depth (mbsf)	TOC (wt%) MD161-7	Depth (mbsf)	TOC (wt%) MD161-8	Depth (mbsf)	TOC (wt%) MD161-10	Depth (mbsf)	TOC (wt%) MD161- 11	Depth (mbsf)	TOC (wt%) MD161-13
0.1	1.3	0.36	1.0	0.05	1.1	0.05	1.2	0.71	1.3	0.71	1.3	0.05	1.0
0.3	1.4	1.71	1.4	0.25	1.0	1.05	1.2	1.21	1.3	1.21	1.4	0.68	1.1
1.4	1.5	2.21	1.3	0.51	1.0	2.05	1.5	2.21	1.3	2.21	1.3	0.83	1.0
1.7	1.4	3.96	1.7	1.01	1.0	3.05	1.6	3.71	1.4	2.71	1.4	1.555	1.3
2.1	1.5	4.96	1.8	1.55	1.1	4.05	1.7	4.21	1.4	3.71	1.4	1.73	1.0
2.6	1.6	5.96	1.9	3.05	1.2	5.05	1.9	5.21	1.8	4.21	1.5	2.18	1.3
2.8	1.7	6.36	2.1	3.25	1.3	6.05	1.9	6.71	1.9	5.21	1.5	3.055	1.3
3.2	1.7	7.36	1.7	3.51	1.4	7.05	1.6	7.21	1.9	5.71	1.6	3.38	1.1
3.4	2.0	8.46	1.3	3.75	1.2	8.05	1.7	8.61	2.0	6.71	1.6	4.535	1.2
3.9	1.8	8.96	1.3	4.01	1.5	9.05	1.2	9.61	1.7	7.21	1.7	6.23	1.3
4.2	1.9	9.36	1.1	4.25	1.2	10.05	1.4	10.11	1.7	8.11	1.7	7.535	1.7
4.5	1.8	9.86	1.9	4.55	1.4	11.05	1.4	11.21	1.7	8.61	2.0	9.055	1.6
4.7	2.1	10.36	1.4	4.75	1.4	12.05	1.6	12.61	1.8	11.51	2.0	12.055	1.8
5	1.8	11.46	1.6	5.01	1.3	13.05	1.8	13.11	1.8	11.71	2.0	13.535	1.9
5.15	2.1	11.96	1.8	5.25	1.3	14.05	1.6	14.71	1.5	12.71	1.6	15.055	1.7
5.3	2.0	12.86	1.4	5.51	1.3	15.05	1.7	15.61	1.6	13.21	1.5	16.535	1.9
5.45	2.0	13.36	1.8	5.75	1.3	16.05	1.7	16.11	1.3	14.11	1.4	18.055	2.1
6	1.8	13.86	1.4	6.05	1.6	17.05	1.3	17.11	1.8	14.61	2.2	19.555	1.1
6.16	2.0	14.46	1.5	6.25	1.5	18.05	1.5	18.71	1.9	15.86	2.0	24.055	1.9
6.31	2.1	15.46	1.4	7.55	1.4	19.05	1.4	19.21	2.0	16.21	2.1	27.055	1.9
6.46	2.2	15.46	1.4	8.25	1.5	21.05	1.4	20.11	1.9	17.11	2.0		
6.61	2.1	15.96	1.4	8.51	1.5	21.42	1.5	21.71	2.0	17.61	2.0		
6.8	1.7	16.46	1.5	8.75	1.7	22.05	1.4	22.21	2.0	18.71	2.0		
7	1.8	16.96	1.5	9.05	1.6	23.05	1.4	23.4	1.9	19.21	2.0		
7.15	1.9	17.46	1.2	9.25	1.5	24.05	1.8			20.11	2.1		
7.3	1.8	17.96	1.1	9.75	1.8	24.42	1.8			20.61	2.1		
7.31	1.7	18.36	1.9	10.25	1.7	25.05	1.8			21.71	2.0		
7.45	1.5			10.55	1.7	25.32	2.0			22.21	2.0		
7.6	1.6			10.75	1.7	26.05	1.9			23.71	1.6		
7.61	2.1			11.01	1.7	27.05	1.8			24.71	1.9		
7.65	2.1			11.51	1.7	29.05	1.7			25.21	2.0		
7.75	1.7			11.75	1.7	29.45	1.9			26.21	2.0		
7.76	1.6			12.05	1.8	30	1.8			26.51	2.0		
7.85	1.4			12.25	1.8					27.45	2.0		

TOC (wt%)		TOC (wt%)	
Depth (mbsf)	MD161-1	Depth (mbsf)	MD161-7
7.86	1.5	12.51	1.7
8	1.4	12.75	1.7
8.15	1.6	13.25	1.7
8.3	1.7	13.55	1.7
8.3	1.7	15.05	1.8
8.45	1.5	16.55	1.8
8.6	1.9	18.05	2.0
8.75	2.0	19.55	2.1
9	1.8	21.05	2.0
9.15	2.0		
9.45	1.4		
9.6	1.3		
9.75	2.0		
9.85	2.2		
9.85	2.2		
10.14	1.7		
10.19	1.7		
10.3	2.0		
10.45	2.0		
10.6	2.0		
10.75	1.7		
10.85	1.7		
11.25	1.8		
11.3	1.3		
11.45	1.9		
11.6	2.5		
11.75	2.3		
11.85	1.9		
12	2.2		
12.15	2.4		
12.3	2.2		
12.45	2.0		
12.6	2.1		
12.75	2.1		
12.85	1.8		
13	2.3		

<b>Depth (mbsf)</b>	<b>MD161-1</b>
13.05	2.2
13.15	2.0
13.45	1.9
13.6	2.3
13.75	2.0
13.9	2.0
14	2.0
14.16	2.1
14.31	2.0
14.46	1.9
14.61	1.8
14.75	1.9
15	1.9
15.16	2.0
15.31	1.5
15.46	1.8
15.61	1.8
15.76	2.4
15.91	2.0
16	1.7
16.16	1.8
16.31	1.4
16.46	2.1
16.61	1.9
16.76	1.9
16.91	2.1
17	1.9
17.15	1.8
17.16	1.9
17.46	2.0
18	1.8
18.16	2.0
18.31	1.9
18.61	2.5
18.76	2.5
18.91	1.6
20	2.1

---